

Exchange Current Operators and Electromagnetic Dipole Transitions in Heavy Quarkonia

T.A. Lähde ^{*}

*Helsinki Institute of Physics and Department of Physical Sciences,
PL 64 University of Helsinki, 00014 Finland*

Abstract

The electromagnetic E1 and M1 transitions in heavy quarkonia ($c\bar{c}, b\bar{b}, c\bar{b}$) and the magnetic moment of the B_c^\pm are calculated within the framework of the covariant Blankenbecler-Sugar (BSLT) equation. The aim of this paper is to study the effects of two-quark exchange current operators which involve the $Q\bar{Q}$ interaction, that arise in the BSLT (or Schrödinger) reduction of the Bethe-Salpeter equation. These are found to be small for E1 dominated transitions such as $\psi(nS) \rightarrow \chi_{cJ} \gamma$ and $\Upsilon(nS) \rightarrow \chi_{bJ} \gamma$, but significant for the M1 dominated ones. It is shown that a satisfactory description of the empirical data on E1 and M1 transitions in charmonium and bottomonium requires unapproximated treatment of the Dirac currents of the quarks. Finally, it is demonstrated that many of the transitions are sensitive to the form of the $Q\bar{Q}$ wavefunctions, and thus require a realistic treatment of the large hyperfine splittings in the heavy quarkonium systems.

^{*}e-mail: talahde@pcu.helsinki.fi

1 Introduction

The radiative decays of heavy quarkonia ($c\bar{c}$, $b\bar{b}$, $c\bar{b}$) have drawn much interest, as they can provide direct information on both the heavy quarkonium wavefunctions and the $Q\bar{Q}$ interaction. Theoretical descriptions range from potential models [1] - [5], QCD sum rules [6, 7], Heavy Quark Effective Theory (HQET) [8] to Non-Relativistic QCD (NRQCD) [9]. As experimental data of a reasonable quality exists for a number of transitions in the $c\bar{c}$ and $b\bar{b}$ systems [10, 11], a fair assessment of the quality of model predictions is already possible. The measured γ decays in the charmonium ($c\bar{c}$) system include the E1 transitions $\chi_{cJ} \rightarrow J/\psi \gamma$ and $\psi' \rightarrow \chi_{cJ} \gamma$, as well as the spin-flip M1 transitions $J/\psi \rightarrow \eta_c \gamma$ and $\psi' \rightarrow \eta_c \gamma$. The situation in the bottomonium ($b\bar{b}$) system is, however, less satisfactory as the total widths of the χ_{bJ} states are not known, and none of the spin-flip M1 decays observed.

Previous calculations of the widths for E1 transitions in heavy quarkonia [1, 3, 12] have achieved qualitative agreement with experiment. However, the situation concerning the M1 transitions has remained unsatisfactory for a long time [13] as the width for $J/\psi \rightarrow \eta_c \gamma$ has typically been overpredicted by a factor of ~ 3 . Calculations of M1 widths using the nonrelativistic Schrödinger equation [3, 14] have demonstrated that the M1 transitions in charmonium are sensitive both to the relativistic aspects of the spin-flip operator as well as the Lorentz structure of the $Q\bar{Q}$ interaction. The results obtained in ref. [14] suggest that a scalar confining interaction may explain the observed width of ~ 1 keV for $J/\psi \rightarrow \eta_c \gamma$, provided that an unapproximated expression for the single quark spin-flip operator is used. However, as many of the M1 transitions are very sensitive to the exact form of the spin-flip operator and the $Q\bar{Q}$ wavefunctions, a more realistic model for the wavefunctions of heavy quarkonia is called for.

This paper reports a comprehensive calculation of the E1 and M1 transitions in heavy quarkonia, as well as the magnetic moment of the B_c^\pm ($c\bar{b}$, $b\bar{c}$) meson, within the framework of the covariant Blankenbecler-Sugar (BSLT) equation [16]. The $Q\bar{Q}$ interaction Hamiltonian is formed of scalar confining and vector one-gluon exchange (OGE) components, in addition to a small instanton induced interaction [17]. The hyperfine components of the $Q\bar{Q}$ interaction have been fully taken into account, which is found to be important for several E1 and M1 transitions, in line with the conclusion reached in ref. [18]. On the other hand, the elimination of the negative energy components of the Bethe-Salpeter equation leads to the appearance of two-quark transition operators [19]. These exchange current operators, which depend explicitly on the Lorentz coupling structure of the $Q\bar{Q}$ interaction, have been shown to give large corrections to the single quark transition operators [14, 20].

The aim of this paper is to evaluate the exchange current contributions to the electric and magnetic dipole operators for the $Q\bar{Q}$ interaction Hamiltonian described above. The contributions from exchange charge operators to the E1 transition rates are shown to be highly suppressed by the large masses of the charm and bottom quarks. However, it is found that the exchange magnetic moment operator associated with the scalar confining component of the $Q\bar{Q}$ interaction gives a large contribution, which makes it possible to bring the calculated width for $J/\psi \rightarrow \eta_c \gamma$ into agreement with the observed width of ~ 1 keV. It is also found that the empirical width of ~ 1 keV for the forbidden transition $\psi' \rightarrow \eta_c \gamma$ may be similarly explained if a relativistic single-quark spin-flip operator is employed together with wavefunctions that model the spin-spin splitting of the ψ states. This provides evidence in favor of a dominant scalar Lorentz structure for the effective linear confining interaction, as an effective vector interaction gives a vanishing contribution to the spin-flip operator for M1 transitions in the $c\bar{c}$ and $b\bar{b}$ systems [14]. On the other hand, for the B_c^\pm the OGE interaction contributes an exchange magnetic moment operator that counteracts that from the scalar confining interaction.

The layout of this paper is as follows: Section 2 presents the transition operators for E1 and M1 decay, while section 3 deals with the Hamiltonian model and $Q\bar{Q}$ wavefunctions, along with formulas for the E1 and M1 widths. Section 4 presents the numerical results for the radiative decays and the B_c^\pm magnetic moment, and section 5 contains a discussion of the obtained results.

2 The Electric Dipole and Magnetic Moment Operators

2.1 The Charge Density and Electric Dipole Operators

From the S -matrix element for one-photon emission by a two-quark system,

$$S_{fi} = -i \langle f | \delta_1 \delta_2 \hat{\varepsilon}_\mu J_\mu | i \rangle, \quad (1)$$

where $\delta_{1,2}$ are four-momentum conserving delta functions for quarks 1 and 2, and J_μ is the current operator of the two-quark system, the electromagnetic transition amplitude for $Q\bar{Q}$ systems is obtained, in the impulse approximation, as

$$T_{fi} = - \int d^3 r_1 d^3 r_2 \varphi_f^*(\vec{r}_1, \vec{r}_2) \hat{\varepsilon} \cdot [e^{i\vec{q} \cdot \vec{r}_1} \vec{j}_1(\vec{q}) + e^{i\vec{q} \cdot \vec{r}_2} \vec{j}_2(\vec{q})] \varphi_i(\vec{r}_1, \vec{r}_2), \quad (2)$$

where \vec{q} and $\hat{\varepsilon}$ denote the momentum and polarization of the emitted photon, respectively, while φ_i and φ_f denote the orbital wavefunctions of the initial and final heavy quarkonium states. In the above equation, \vec{j}_1 and \vec{j}_2 denote the single quark current operators of quarks 1 and 2, respectively. Note that the current operator $\vec{j}(\vec{q})$ corresponds to the quantity in square brackets in eq. (2). The amplitude for a γ transition is then

$$T_{fi} = i |\vec{q}| \int d^3 r_1 d^3 r_2 \varphi_f^*(\vec{r}_1, \vec{r}_2) \hat{\varepsilon} \cdot \vec{d}(\vec{r}_1, \vec{r}_2) \varphi_i(\vec{r}_1, \vec{r}_2), \quad (3)$$

where the dipole operator $\vec{d}(\vec{r}_1, \vec{r}_2)$ is of the form

$$\vec{d}(\vec{r}_1, \vec{r}_2) = \int d^3 r' e^{i\vec{q} \cdot \vec{r}'} \vec{r}' \rho(\vec{r}', \vec{r}_1, \vec{r}_2). \quad (4)$$

In order to distinguish the above model from the rigorous E1 approximation, it will be referred to as "dynamical" throughout this paper. The E1 approximation is then obtained in the limit $\vec{q} \rightarrow 0$. If contributions to the charge operator $\rho(\vec{r}', \vec{r})$, that are proportional to higher powers of the photon momentum are to be included, then the usefulness of the dynamical model is apparent. More significantly, the dynamical model allows the recoil of the heavy meson to be accounted for.

The charge density operator $\rho(\vec{r}')$ contains, in addition to the single quark contribution ρ_{sq} , an exchange part ρ_{ex} , which arises from processes that are illustrated by the diagrams shown in Fig. 1. These contributions arise from the elimination of the negative energy components in the reduction of the Bethe-Salpeter equation to a BSLT (or Schrödinger) equation. An obvious constraint is that two-quark contributions to the charge density should have vanishing volume integrals.

Consider first the single quark charge operator $\rho_{sq}(\vec{r}', \vec{r}) = \rho_1(\vec{r}', \vec{r}_1) + \rho_2(\vec{r}', \vec{r}_2)$. The corresponding dipole operator may be expressed as

$$\vec{d}_{sq}(\vec{r}_1, \vec{r}_2) = Q_1 \vec{r}_1 e^{i\vec{q}_f \cdot \vec{r}_1} + Q_2 \vec{r}_2 e^{i\vec{q}_f \cdot \vec{r}_2}, \quad (5)$$

where Q_1 and Q_2 are the appropriate electric charges of the constituent charm and bottom quarks. Note that Q_1 is taken to be the charge of the heavy quark, while Q_2 denotes that of the heavy antiquark. Relativistic modifications to the above expression will be considered further on. Insertion of eq. (5) into eq. (3) yields the amplitude

$$T_{fi} = i |\vec{q}_f| (2\pi)^3 \delta^3(P_f - P_i - q_f) \int d^3 r \varphi_f^*(\vec{r}) \hat{\varepsilon} \cdot \vec{d}(\vec{r}) \varphi_i(\vec{r}), \quad (6)$$

where $\vec{r} = \vec{r}_1 - \vec{r}_2$, to which the contribution from the single quark dipole operator (5) is

$$\vec{d}_{\text{sq}}(\vec{r}) = \left[\frac{Q_1 m_2 - Q_2 m_1}{m_1 + m_2} \right] \vec{r} e^{i\vec{q}_f \cdot \vec{r}/2}, \quad (7)$$

where $\vec{r} = \vec{r}_1 - \vec{r}_2$. Again, the E1 expression [5] is obtained by dropping the exponential in eq. (7) and setting $\vec{q}_f = 0$ in the delta function in eq. (6). Note that for the $c\bar{c}$ and $b\bar{b}$ systems, the factor in brackets in eq. (7) reduces to the charge of the charm and bottom quark, respectively.

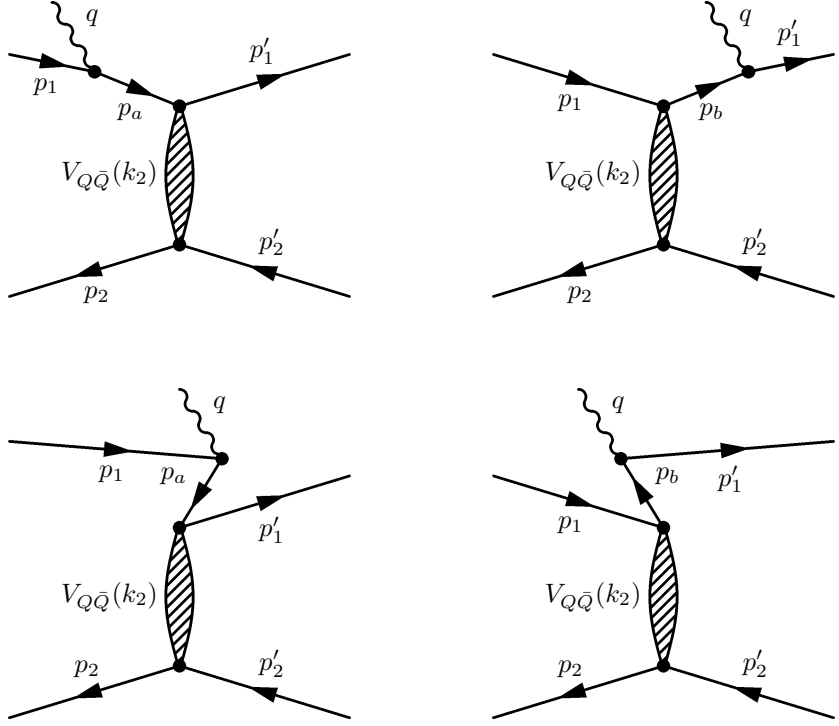


Figure 1: Relativistic Born diagrams for photon emission by a heavy constituent quark. The lower diagrams describe the negative energy components of the upper diagrams, and can be obtained from the latter by separation of the intermediate quark propagators p_a and p_b into negative and positive energy components. Note that similar diagrams describe photon emission by the heavy antiquark. The exchange charge operators that correspond to the above diagrams have been calculated for different Lorentz coupling structures of the interaction V in ref. [21], which in the case of the $Q\bar{Q}$ interaction will contain scalar confining and vector OGE components.

Consider next the two-quark exchange charge operators from the Born diagrams given in Fig. 1. If those operators are decomposed according to $\rho_{\text{ex}}(\vec{r}', \vec{r}_1, \vec{r}_2) = \rho_{\text{ex1}}(\vec{r}', \vec{r}_1) + \rho_{\text{ex2}}(\vec{r}', \vec{r}_2)$, then the exchange charge contribution to the two-quark dipole operator

$$\vec{d}_{\text{ex}}(\vec{r}_1, \vec{r}_2) = \int d^3 r' e^{i\vec{q}_f \cdot \vec{r}'} \vec{r}' \rho_{\text{ex}}(\vec{r}', \vec{r}_1, \vec{r}_2) \quad (8)$$

may be expressed as

$$\vec{d}_{\text{ex1}}(\vec{r}_1) = \vec{r}_1 e^{i\vec{q}_f \cdot \vec{r}_1} \int \frac{d^3 k_2}{(2\pi)^3} e^{-i\vec{k}_2 \cdot \vec{r}} \rho_{\text{ex1}}(\vec{q}_f, \vec{k}_2) - \lim_{q \rightarrow q_f} \left[e^{i\vec{q} \cdot \vec{r}_1} i\nabla_{\vec{q}} \int \frac{d^3 k_2}{(2\pi)^3} e^{-i\vec{k}_2 \cdot \vec{r}} \rho_{\text{ex1}}(\vec{q}, \vec{k}_2) \right], \quad (9)$$

from which the E1 approximation can again be obtained by setting $q_f \rightarrow 0$.

Having established eq. (9), the relativistic modifications to the single quark charge operator as well as the two-quark exchange charge operators from Fig. 1 may be considered. To second order in v/c , the single quark charge operator may be expressed in the form [21]

$$\rho_{\text{sq}} \simeq Q_1 \left[1 - \frac{\vec{q}^2}{8m^2} + \frac{i\vec{\sigma}_1 \cdot \vec{p}'_1 \times \vec{p}_1}{4m^2} \right] + (1 \rightarrow 2), \quad (10)$$

where it is understood that the contribution from quark 2 is obtained by replacing the indices accordingly. The second term on the r.h.s. is the relativistic Darwin-Foldy term. It will be shown that the effect of this term is very small because of the large masses of the heavy constituent quarks. Note that this expansion is justified by the small coefficient of the q^2 term; It has been shown in ref. [14] that such an expansion cannot be used for the magnetic moment operator. The spin-orbit term in eq. (10) is linear in the photon momentum \vec{q} and will be left out in this work because of its smallness. For transitions between S -wave states, this term vanishes entirely [21]. Note that in the E1 approximation, the contribution from the Darwin-Foldy term to the dipole operator will likewise vanish.

The exchange charge density operators that are associated with the $Q\bar{Q}$ interaction have been calculated in ref. [21], where the appropriate operators were extracted for different Lorentz invariants for systems composed of quarks with equal masses. When generalized to the case of unequal quark masses, the required operators are obtained as

$$\rho_{\text{ex}}^c = \frac{Q_1}{4m_1^3} q^2 V_c(\vec{k}_2) + \frac{Q_2}{4m_2^3} q^2 V_c(\vec{k}_1) \quad (11)$$

for the scalar confining interaction, and

$$\rho_{\text{ex}}^g = \frac{Q_1}{4m_1^2} \left[\frac{\vec{q} \cdot \vec{k}_2}{m_1} + \frac{2}{3} \frac{\vec{q} \cdot \vec{k}_2 \vec{\sigma}_1 \cdot \vec{\sigma}_2}{m_2} \right] V_g(\vec{k}_2) + \frac{Q_2}{4m_2^2} \left[\frac{\vec{q} \cdot \vec{k}_1}{m_2} + \frac{2}{3} \frac{\vec{q} \cdot \vec{k}_1 \vec{\sigma}_1 \cdot \vec{\sigma}_2}{m_1} \right] V_g(\vec{k}_1) \quad (12)$$

for the vector coupled OGE interaction. In the above expressions, V_c and V_g denote the momentum space forms of the confining and OGE interactions, respectively. Note that the terms in eqs. (11) and (12) that depend on \vec{k}_2 correspond to the contribution ρ_{ex1} in eq. (9) and vice versa. In the E1 approximation, the contribution to the dipole operator from eq. (11) vanishes, while in the dynamical model, evaluation of eq. (9) yields, analogously to eq. (7),

$$\vec{d}_{\text{ex}}^{\text{Conf}}(\vec{r}) = q_f^2 \left[\frac{Q_1}{4m_1^3} \frac{m_2}{m_1 + m_2} - \frac{Q_2}{4m_2^3} \frac{m_1}{m_1 + m_2} \right] \vec{r} V_c(r) e^{i\vec{q}_f \cdot \vec{r}/2}, \quad (13)$$

where the scalar confining interaction is of the form $V_c(r) = cr$. Note that the second term in eq. (9) vanishes because $\vec{q} \cdot \hat{e} = 0$. On the other hand, the OGE expression (12) gives a contribution, the dominant term of which is

$$\vec{d}_{\text{ex}}^{\text{Oge}}(\vec{r}) = \left[\frac{Q_1}{4m_1^2} \left(\frac{1}{m_1} + \frac{2}{3} \frac{\vec{\sigma}_1 \cdot \vec{\sigma}_2}{m_2} \right) - \frac{Q_2}{4m_2^2} \left(\frac{1}{m_2} + \frac{2}{3} \frac{\vec{\sigma}_1 \cdot \vec{\sigma}_2}{m_1} \right) \right] \vec{r} \left(\frac{\partial V_g(r)}{r \partial r} \right) e^{i\vec{q}_f \cdot \vec{r}/2}. \quad (14)$$

Here $V_g(r)$ denotes the form of the OGE interaction in configuration space, and is here taken to be the Fourier transform of eq. (32). This choice allows the inclusion of the running coupling of QCD. Note that eq. (14) gives a non-vanishing contribution also in the E1 approximation.

2.2 The Current Density and Magnetic Moment Operators

In the impulse approximation, the spin-flip magnetic moment operator for M1 transitions between S -wave heavy quarkonium states may be obtained from the amplitude

$$T_{fi} = -(2\pi)^3 \delta^3(P_f - P_i - q_f) \int d^3r \varphi_f^*(\vec{r}) \hat{\varepsilon} \cdot \left[e^{i\vec{q}\cdot\vec{r}/2} \vec{j}_1(\vec{q}) + e^{-i\vec{q}\cdot\vec{r}/2} \vec{j}_2(\vec{q}) \right] \varphi_i(\vec{r}), \quad (15)$$

where $\vec{r} = \vec{r}_1 - \vec{r}_2$. The corresponding matrix element for an M1 transition may be written in the form

$$\mathcal{M}_{fi} = i \int d^3r \varphi_f^*(\vec{r}) \vec{q} \times \hat{\varepsilon} \cdot \vec{\mu}_{\text{sf}} \varphi_i(\vec{r}), \quad (16)$$

where $\vec{\mu}_{\text{sf}}$ denotes the spin-flip part of the standard magnetic moment operator. In addition to the single quark current operators in eq. (15), the negative energy Born diagrams in Fig. 1 contribute a two-quark current operator \vec{j}_{ex} . Decomposition of the single quark current into contributions from quark 1 and 2 according to $\vec{j}_{\text{sq}} = \vec{j}_1 + \vec{j}_2$ yields the magnetic moment operator

$$\vec{\mu}_{\text{sq}} = \lim_{\vec{q} \rightarrow 0} \left[-\frac{i}{2} \nabla_q \times \left(e^{i\vec{q}\cdot\vec{r}/2} \vec{j}_1(\vec{q}) + e^{-i\vec{q}\cdot\vec{r}/2} \vec{j}_2(\vec{q}) \right) \right], \quad (17)$$

in the nonrelativistic impulse approximation (NRIA). However, previous work has demonstrated that the static magnetic moment operators of the baryons are significantly modified by the canonical boosts of the constituent quark spinors [23, 24]. In ref. [14], it was shown that the static spin-flip magnetic moment operators for M1 decay of $Q\bar{Q}$ states are also significantly affected, despite the large masses of the charm and bottom constituent quarks.

The matrix element that corresponds to eq. (16) in the relativistic impulse approximation (RIA) may be obtained as

$$\mathcal{M}_{fi}^{\text{Rel}} = i \int \frac{d^3P}{(2\pi)^3} d^3r d^3r' e^{i\vec{P}\cdot(\vec{r}'-\vec{r})} \varphi_f^*(\vec{r}') \vec{q} \times \hat{\varepsilon} \cdot \vec{\mu}_{\text{sq}}^{\text{Rel}}(\vec{P}) \varphi_i(\vec{r}), \quad (18)$$

where the final and initial state coordinates \vec{r}' and \vec{r} are defined as $\vec{r}'_1 - \vec{r}'_2$ and $\vec{r}_1 - \vec{r}_2$ respectively. In eq. (18), the momentum variable \vec{P} is defined as $\vec{P} = (\vec{p}' + \vec{p})/2$, where \vec{p}' and \vec{p} are the relative momenta in the representation $\vec{p}_1 = \vec{P}_i/2 + \vec{p}$, $\vec{p}_2 = \vec{P}_i/2 - \vec{p}$ and $\vec{p}'_1 = \vec{P}_f/2 + \vec{p}'$, $\vec{p}'_2 = \vec{P}_f/2 - \vec{p}'$. The relativistic single quark magnetic moment operator that appears in the matrix element (18) can be obtained from eq. (17) by the substitution $\vec{r} \rightarrow (\vec{r}' + \vec{r})/2$.

In the nonrelativistic case, the spin-dependent part of the single quark current operator $\vec{j}_{\text{sq}} = \vec{j}_1 + \vec{j}_2$ is of the form

$$\vec{j}_{\text{sq}}^{\text{spin}} = \frac{ie}{2} (\vec{\sigma}_1 + \vec{\sigma}_2) \times \vec{q} \left[\frac{Q_1}{2m_1} + \frac{Q_2}{2m_2} \right] + \frac{ie}{2} (\vec{\sigma}_1 - \vec{\sigma}_2) \times \vec{q} \left[\frac{Q_1}{2m_1} - \frac{Q_2}{2m_2} \right]. \quad (19)$$

The first term, which vanishes for equal mass quarkonia, describes the magnetic moment of the two-quark system whereas the second term is the spin-flip operator for M1 decay in the nonrelativistic impulse approximation (NRIA). The corresponding spin-flip operator in the relativistic impulse approximation (RIA) has been calculated in refs. [24, 20], and may for transitions between S -wave states be expressed as

$$\vec{\mu}_{\text{sq}}^{\text{Rel}} = \frac{e}{2} \left[\frac{Q_1}{2m_1} f_1^\gamma - \frac{Q_2}{2m_2} f_2^\gamma \right] (\vec{\sigma}_1 - \vec{\sigma}_2), \quad f_i^\gamma = \frac{m_i}{3E_i} \left[2 + \frac{m_i}{E_i} \right], \quad (20)$$

with $E_i = \sqrt{P^2 + m_i^2}$. It is apparent from the above expression that the relativistic treatment will effectively weaken the NRIA result.

The relativistic Born diagrams in Fig. 1 contribute significant two-quark exchange currents that give rise to two-quark magnetic moment operators [22]. This situation is akin to that for the magnetic moments of the baryons [23, 24], but in that case additional complications arise from flavor dependent meson exchange interactions. Decomposition of the exchange current operator according to $\vec{j}_{\text{ex}}(\vec{q}, \vec{k}_1, \vec{k}_2) = \vec{j}_{\text{ex1}}(\vec{q}, \vec{k}_2) + \vec{j}_{\text{ex2}}(\vec{q}, \vec{k}_1)$ yields the exchange magnetic moment operator

$$\vec{\mu}_{\text{ex}} = \lim_{\vec{q} \rightarrow 0} \left[-\frac{i}{2} \nabla_{\vec{q}} \times \left(e^{i\vec{q} \cdot \vec{r}/2} \int \frac{d^3 k_2}{(2\pi)^3} e^{-i\vec{k}_2 \cdot \vec{r}} \vec{j}_{\text{ex1}}(\vec{q}, \vec{k}_2) + e^{-i\vec{q} \cdot \vec{r}/2} \int \frac{d^3 k_1}{(2\pi)^3} e^{i\vec{k}_1 \cdot \vec{r}} \vec{j}_{\text{ex2}}(\vec{q}, \vec{k}_1) \right) \right]. \quad (21)$$

However, the exchange magnetic moment operators turn out to be difficult to calculate directly from the above equation. Instead, they can be conveniently extracted from the expression [22]

$$\vec{\mu}_{\text{ex}} = \lim_{\vec{q} \rightarrow 0} \left[-\frac{i}{2} \int \frac{d^3 k}{(2\pi)^3} e^{-i\vec{k} \cdot \vec{r}} \nabla_{\vec{q}} \times \left\{ \vec{j}_{\text{ex1}} \left(\frac{\vec{q}}{2} + \vec{k} \right) + \vec{j}_{\text{ex2}} \left(\frac{\vec{q}}{2} - \vec{k} \right) \right\} \right], \quad (22)$$

where $\vec{k}_2 = \vec{k} + \vec{q}/2$ and $\vec{k}_1 = -\vec{k} + \vec{q}/2$. By means of eq. (22), it is now possible to consider the two-quark current operators for the scalar confining and vector OGE interactions, as calculated from the diagrams in Fig. 1 by refs. [20, 22]. The two-quark current operator associated with the scalar confining interaction is of the form

$$\vec{j}_{\text{ex}}^{\text{c}} = -e \left(\frac{Q_1^* \vec{P}_1}{m_1^2} + \frac{Q_2^* \vec{P}_2}{m_2^2} + \frac{i}{2} (\vec{\sigma}_1 + \vec{\sigma}_2) \times \vec{q} \left[\frac{Q_1^*}{2m_1^2} + \frac{Q_2^*}{2m_2^2} \right] + \frac{i}{2} (\vec{\sigma}_1 - \vec{\sigma}_2) \times \vec{q} \left[\frac{Q_1^*}{2m_1^2} - \frac{Q_2^*}{2m_2^2} \right] \right), \quad (23)$$

in which case the two-quark magnetic moment operator is most conveniently computed using eq. (21), as the spin part of eq. (23) depends explicitly on the photon momentum \vec{q} . In the above equation, the variables Q_1^* and Q_2^* are defined as $Q_1^* = V_c(\vec{k}_2)Q_1$ and $Q_2^* = V_c(\vec{k}_1)Q_2$, respectively. The corresponding current operator for the OGE interaction may be expressed as

$$\vec{j}_{\text{ex}}^{\text{g}} = -e \left(Q_1^* \left[\frac{i\vec{\sigma}_1 \times \vec{k}_2}{2m_1^2} + \frac{2\vec{P}_2 + i\vec{\sigma}_2 \times \vec{k}_2}{2m_1 m_2} \right] + Q_2^* \left[\frac{i\vec{\sigma}_2 \times \vec{k}_1}{2m_2^2} + \frac{2\vec{P}_1 + i\vec{\sigma}_1 \times \vec{k}_1}{2m_1 m_2} \right] \right), \quad (24)$$

with $Q_1^* = V_g(\vec{k}_2)Q_1$ and $Q_2^* = V_g(\vec{k}_1)Q_2$. As the above equation depends only on \vec{k}_1 and \vec{k}_2 , the OGE magnetic moment operator is most conveniently calculated using eq. (22). By Fourier transformation, the resulting magnetic moment operators for transitions between S -wave quarkonium states may be obtained as [20]

$$\vec{\mu}_{\text{ex}}^{\text{Conf}} = -\frac{eV_c(r)}{4} \left\{ \left[\frac{Q_1}{m_1^2} - \frac{Q_2}{m_2^2} \right] (\vec{\sigma}_1 - \vec{\sigma}_2) + \left[\frac{Q_1}{m_1^2} + \frac{Q_2}{m_2^2} \right] (\vec{\sigma}_1 + \vec{\sigma}_2) \right\} \quad (25)$$

for the scalar confining interaction, and

$$\vec{\mu}_{\text{ex}}^{\text{Oge}} = -\frac{eV_g(r)}{8} \left\{ \left[\frac{Q_1}{m_1^2} - \frac{Q_2}{m_2^2} - \frac{Q_1 - Q_2}{m_1 m_2} \right] (\vec{\sigma}_1 - \vec{\sigma}_2) + \left[\frac{Q_1}{m_1^2} + \frac{Q_2}{m_2^2} + \frac{Q_1 + Q_2}{m_1 m_2} \right] (\vec{\sigma}_1 + \vec{\sigma}_2) \right\} \quad (26)$$

for the OGE interaction. For equal constituent quark masses, eqs. (25) and (26) reduce to the expressions given in ref. [22]. Note that the presence of a spin-flip term in the OGE operator (26) is solely a consequence of the difference in mass between the constituent quarks, and will thus not contribute to the M1 decay widths of the charmonium and bottomonium states. Similarly, the terms that are symmetric in the quark spins vanish for equal mass quarkonia. However, in the case of the B_c^\pm system, these terms will contribute to the magnetic moment of the $c\bar{b}$ system. Also the spin-flip M1 decays in the B_c^\pm system will receive a contribution from the OGE operator.

3 Wavefunctions and Decay Widths

3.1 Hamiltonian model

The interaction Hamiltonian employed in this paper for the $Q\bar{Q}$ interaction contains contributions from the scalar confining, the vector one-gluon exchange (OGE), and the instanton induced interaction of ref. [17]. This Hamiltonian is thus of the form

$$H_{\text{int}} = V_{\text{Conf}} + V_{\text{Oge}} + V_{\text{Inst}}, \quad (27)$$

and has been employed together with the covariant Blankenbecler-Sugar (BSLT) equation. That equation may be expressed as an eigenvalue equation of the form

$$(H_0 + H_{\text{int}})\Psi_{\text{nlm}}(\vec{r}) = \varepsilon(E, M_Q, M_{\bar{Q}})\Psi_{\text{nlm}}(\vec{r}), \quad (28)$$

where H_0 denotes the kinetic energy operator of the nonrelativistic Schrödinger equation and the eigenvalue $\varepsilon(E, M_Q, M_{\bar{Q}})$ is a quadratic mass operator [15] which is related to the energy E of the heavy quarkonium state according to

$$\varepsilon = \frac{[E^2 - (M_Q + M_{\bar{Q}})^2][E^2 - (M_Q - M_{\bar{Q}})^2]}{8\mu E^2} \quad (29)$$

where μ is the reduced mass of the quark-antiquark system. As the details of the interaction Hamiltonian (27) have already been described in ref. [15], only the main points will be repeated here. The interaction operators V in eq. (27), which in general are nonlocal, may be obtained from the $Q\bar{Q}$ irreducible quasipotential \mathcal{V} according to

$$V(\vec{p}', \vec{p}) = \sqrt{\frac{M_Q + M_{\bar{Q}}}{W(\vec{p}')}} \mathcal{V}(\vec{p}', \vec{p}) \sqrt{\frac{M_Q + M_{\bar{Q}}}{W(\vec{p})}}, \quad (30)$$

where the function W is defined as $W(\vec{p}) = E_Q(\vec{p}) + E_{\bar{Q}}(\vec{p})$ with $E_i(\vec{p}) = \sqrt{M_i^2 + \vec{p}^2}$. Note that in the Born approximation the quasipotential \mathcal{V} is set equal to the $Q\bar{Q}$ invariant scattering amplitude \mathcal{T} , whereby a constructive relation to field theory obtains.

The OGE interaction in momentum space can be parameterized [25] in terms of the strong coupling $\alpha_s(k^2)$ according to

$$V_{\text{Oge}}(\vec{k}) = -\frac{16\pi}{3} \frac{\alpha_s(\vec{k}^2)}{\vec{k}^2}, \quad \alpha_s(\vec{k}^2) = \frac{12\pi}{27} \ln^{-1} \left[\frac{\vec{k}^2 + 4m_g^2}{\Lambda_{\text{QCD}}^2} \right]. \quad (31)$$

Here Λ_{QCD} denotes the QCD scale of ~ 250 MeV, and m_g is a dynamical gluon mass which determines the low-momentum behavior of α_s . Application of eq. (31) together with eq. (30) yields the central and spin-dependent potential components of the OGE interaction, and are given in ref. [15]. For example, if all higher order nonlocalities are dropped, the central Coulomb component of the OGE interaction is modified to

$$V_{\text{Oge}}(r) = -\frac{4}{3} \frac{2}{\pi} \int_0^\infty dk j_0(kr) \frac{M_Q}{e_Q} \frac{M_{\bar{Q}}}{e_{\bar{Q}}} \left(\frac{M_Q + M_{\bar{Q}}}{e_Q + e_{\bar{Q}}} \right) \alpha_s(k^2), \quad (32)$$

where the factors e_Q and $e_{\bar{Q}}$ are defined as $e_Q = \sqrt{M_Q^2 + k^2/4}$ and $e_{\bar{Q}} = \sqrt{M_{\bar{Q}}^2 + k^2/4}$. If α_s is taken to be constant, then the above form reduces to the Coulombic potential suggested by perturbative QCD

in the limit $M_Q \rightarrow \infty$. On the other hand, the Fourier transform of a linear confining potential of the form $V_{\text{Conf}} = cr$ may be expressed as

$$V_{\text{Conf}}(r) = \lim_{\lambda \rightarrow 0} \int \frac{d^3k}{(2\pi)^3} e^{-i\vec{k} \cdot \vec{r}} \frac{8\pi c}{k^4} \left[\frac{4\lambda^2 k^4}{(\lambda^2 + k^2)^3} - \frac{k^4}{(\lambda^2 + k^2)^2} \right]. \quad (33)$$

For the purpose of calculating the spin-orbit term associated with the scalar confining interaction, the limit $\lambda \rightarrow 0$ may be taken directly to yield $V_{\text{Conf}}(\vec{k}) = -8\pi c/k^4$. Finally the instanton induced interaction is expressed as

$$V_{\text{Inst}}(r) = -\frac{\Delta M_Q \Delta M_{\bar{Q}}}{4n} \int_0^\infty dk k^2 j_0(kr) \left(\frac{M_Q + M_{\bar{Q}}}{e_Q + e_{\bar{Q}}} \right) \frac{M_Q M_{\bar{Q}}}{e_Q e_{\bar{Q}}}, \quad (34)$$

where the notation is similar to that employed in ref. [17]. The parameter ΔM_Q denotes the mass shift of the heavy constituent quark due to the instanton induced interaction, which for a charm quark is of the order ~ 100 MeV [17]. The parameter n represents the instanton density, which is usually taken to be $\sim 1 \text{ fm}^{-4}$. Note that in the limit of infinitely heavy constituent quarks, eq. (34) reduces to a delta function. The above smeared out form is convenient since it allows for direct numerical treatment of the instanton induced interaction with the differential equation (28).

The wavefunctions needed for the calculation of the E1 and M1 widths of the heavy quarkonia are thus taken to be the solutions to eq. (28) obtained in ref. [15]. As the spin-spin interaction in the charmonium system is strong enough to produce a $J/\psi - \eta_c$ splitting of ~ 120 MeV, then the respective radial wavefunctions are likely to show marked differences. Thus the employment of spin-averaged wavefunctions and a perturbative treatment of the spin-dependent hyperfine interaction is undesirable. With this in mind, the hyperfine components of the $Q\bar{Q}$ interaction have been taken fully into account, which is possible since they are nonsingular in the BSLT framework. In particular, it is expected that such effects should be significant for transitions which involve a change in the principal quantum number of the $Q\bar{Q}$ state. The effect of the S -wave spin-spin interaction on the radial wavefunctions is demonstrated by Fig. 2. The calculated spectra of the heavy quarkonia and the model parameters are given in Tables 1 and 2, respectively.

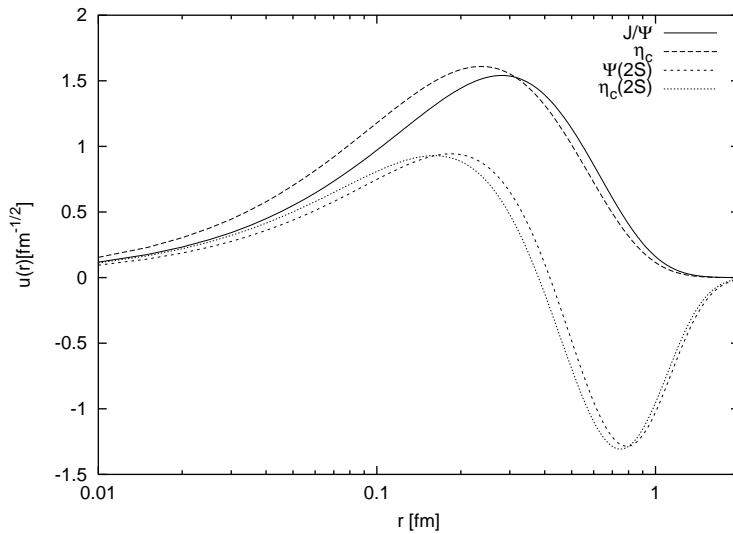


Figure 2: The reduced radial wavefunctions for the charmonium 1S and 2S states, from ref. [15]. The differences between the spin singlet η_c and spin triplet ψ wavefunctions are due to the short-ranged OGE spin-spin interaction. Note that the r axis has been made logarithmic in order to emphasize the short range part of the wavefunctions.

$n^{2S+1}L_J$	$b\bar{b}$	Exp($b\bar{b}$)	$c\bar{c}$	Exp($c\bar{c}$)	$c\bar{b}$
1^1S_0	9401	—	2997	2980 ± 1.8	6308
2^1S_0	10005	—	3640	3654 ± 6 [27]	6888
3^1S_0	10361	—	4015	—	7229
4^1S_0	10634	—	4300	—	7488
1^3S_1	9458	9460	3099	3097	6361
2^3S_1	10030	10023	3678	3686	6910
3^3S_1	10377	10355	4040	4040 ± 10	7244
4^3S_1	10648	10580	4319	4159 ± 20 ?	7500
1^1P_1	9888	—	3513	—	6754
2^1P_1	10266	—	3912	—	7126
3^1P_1	10552	—	4211	—	7401
1^3P_0	9855	9860	3464	3415	6723
2^3P_0	10244	10232	3884	—	7107
3^3P_0	10535	—	4192	—	7387
1^3P_1	9883	9893	3513	3511	6751
2^3P_1	10263	10255	3913	—	7125
3^3P_1	10550	—	4213	—	7400
1^3P_2	9903	9913	3540	3556	6770
2^3P_2	10277	10269	3930	—	7136
3^3P_2	10561	—	4226	—	7410
1^3D_3	10158	—	3790	—	7009
1^3D_2	10149	—	3784	—	7006
1^3D_1	10139	—	3768	3770 ± 2.5	6998

Table 1: Calculated and experimental charmonium, bottomonium and B_c^\pm states rounded to the nearest MeV. The states are classified according to excitation number n , total spin S , total orbital angular momentum L and total angular momentum J . Note that experimental uncertainties are indicated only where they are appreciable. For a graphical plot of the $c\bar{c}$ and $b\bar{b}$ data, see ref. [15]. The $c\bar{c}$ and $b\bar{b}$ values are from ref. [15]. The experimental states correspond to the values reported by ref. [10], except for the recently observed [27] $\eta_c(2S)$. The measured mass of the B_c^\pm was reported in ref. [28] as 6.40 ± 0.39 GeV, which is about ~ 100 MeV higher than the predicted 6308 MeV, and most other models give even lower masses for the B_c^\pm ground state [5]. The predicted B_c^\pm spectrum agrees, however, very well with the QCD-inspired model of ref. [29]. Within the framework of QCD sum rules, the mass of the B_c^\pm has been predicted to be ~ 6.35 GeV [6].

	Ref. [15]	Other sources
M_b	4885 MeV	4870 MeV [30]
M_c	1500 MeV	1530 MeV [30]
Λ_{QCD}	260 MeV	200-300 MeV [25]
m_g	290 MeV	$m_g > \Lambda_{\text{QCD}}$ [25]
c	890 MeV/fm	912 MeV/fm [30]
$\frac{(\Delta M_c)^2}{4n}$	0.084 fm ²	~ 0.05 fm ² [17]
$\frac{(\Delta M_b)^2}{4n}$	0.004 fm ²	—
$\frac{\Delta M_b \Delta M_c}{4n}$	0.018 fm ²	—

Table 2: Constituent quark masses and parameters for the $Q\bar{Q}$ interaction that have been used in the calculation of the spectra presented in Table 1. The heavy masses are close to those preferred by ref. [30], and in general in agreement with the values of previous work. The form of the running QCD coupling α_s is in line with the criteria of refs. [25, 26], and the confining string tension c agrees well with previous calculations [30, 31]. The strength of the instanton induced interaction for $c\bar{c}$ is comparable to the estimate given by ref. [17].

3.2 Widths for radiative decay

The decay width for an E1 dominated transition of the type $\chi_{cJ} \rightarrow J/\psi \gamma$ or $\psi' \rightarrow \chi_{cJ} \gamma$ is given by

$$\Gamma = \mathcal{S}_{fi} \frac{2J_f+1}{3} q^3 \alpha \frac{M_f}{M_i} \left[\frac{4}{9} |\mathcal{M}_0|^2 + \frac{8}{9} |\mathcal{M}_2|^2 \right], \quad (35)$$

where J_f is the total angular momentum of the final quarkonium state, and q is the momentum of the emitted photon. One would thus expect that the widths for $\psi' \rightarrow \chi_{cJ} \gamma$ with $J = 0, 1, 2$ would scale as 1 : 3 : 5 respectively. In practice, however, this result is modified by the large hyperfine splittings in the $L = 1$ heavy quarkonia. The factor \mathcal{S}_{fi} is defined as in ref. [5] and assumes the values $\mathcal{S}_{fi} = 1$ for a triplet-triplet transition and $\mathcal{S}_{fi} = 3$ for a singlet-singlet transition of the type $h_c \rightarrow \eta_c \gamma$. On the other hand, the widths for transitions between D - and P -wave states are calculated according to

$$\Gamma = 4 \mathcal{S}_{fi} \frac{2J_f+1}{27} q^3 \alpha \frac{M_f}{M_i} |\mathcal{M}_0|^2, \quad \mathcal{S}_{fi} = 18 \left\{ \begin{array}{ccc} 2 & 1 & J_d \\ J_p & 1 & 1 \end{array} \right\}^2, \quad (36)$$

where J_d and J_p are the total angular momenta of the D - and P -wave states, respectively. Note that the triangularity of the 6-j symbol requires that $|J_d - J_p| = 1$ or 0. Consequently, transitions that change the value of J by more than one unit are forbidden. In eqs. (35) and (36), \mathcal{M}_0 and \mathcal{M}_2 denote radial matrix elements for S - and D -wave photon emission, respectively. The radial matrix element for S -wave decay receives contributions not only from the impulse approximation, eq. (7), but also from the confinement and OGE operators (13) and (14). That matrix element may thus be expressed as

$$\mathcal{M}_0 = \int_0^\infty dr r u_f(r) u_i(r) j_0 \left(\frac{qr}{2} \right) \left[\langle Q \rangle_{\text{IA}} + q^2 V_c(r) \langle Q \rangle_c + \left(\frac{\partial V_g(r)}{r \partial r} \right) \langle Q \rangle_g \right], \quad (37)$$

where u_i and u_f are the reduced radial wavefunctions for the initial and final heavy quarkonium states. Similarly, the matrix element for D -wave decay is of the form

$$\mathcal{M}_2 = \langle Q \rangle_{\text{ID}} \int_0^\infty dr r u_f(r) u_i(r) j_2 \left(\frac{qr}{2} \right). \quad (38)$$

The contribution from this matrix element is generally very small, and has therefore not been included in eq. (36).

The impulse approximation charge factor $\langle Q \rangle_{\text{IA}}$, and the exchange charge factors $\langle Q \rangle_c$ for the scalar confining interaction and $\langle Q \rangle_g$ for the OGE interaction that appear in eqs. (37) and (38) are of the form

$$\langle Q \rangle_{\text{IA}} = \left[Q_1 \left(1 - \frac{q^2}{8m_1^2} \right) \frac{m_2}{m_1 + m_2} - Q_2 \left(1 - \frac{q^2}{8m_2^2} \right) \frac{m_1}{m_1 + m_2} \right] \quad (39)$$

for the impulse approximation, where the quark charge operators have been multiplied with the Darwin-Foldy terms from eq. (10), and

$$\langle Q \rangle_c = \left[\frac{Q_1}{4m_1^3} \frac{m_2}{m_1 + m_2} - \frac{Q_2}{4m_2^3} \frac{m_1}{m_1 + m_2} \right], \quad (40)$$

$$\langle Q \rangle_g = \left[\frac{Q_1}{4m_1^2} \left(\frac{1}{m_1} + \frac{2 \langle S_f | \vec{\sigma}_1 \cdot \vec{\sigma}_2 | S_i \rangle}{3 m_2} \right) - \frac{Q_2}{4m_2^2} \left(\frac{1}{m_2} + \frac{2 \langle S_f | \vec{\sigma}_1 \cdot \vec{\sigma}_2 | S_i \rangle}{3 m_1} \right) \right], \quad (41)$$

for the confinement and OGE exchange charge contributions, respectively. In the spin dependent terms of eq. (41), S_i and S_f denote the total spins of the initial and final quarkonium states. For triplet-triplet

and singlet-singlet transitions, $\langle S_f | \vec{\sigma}_1 \cdot \vec{\sigma}_2 | S_i \rangle = +1$ and -3 , respectively. The charge factor $\langle Q \rangle_{\text{ID}}$ that appears in eq. (38) is defined according to $\langle Q \rangle_{\text{ID}} = \lim_{q \rightarrow 0} \langle Q \rangle_{\text{IA}}$. This is permissible since the Darwin-Foldy and exchange charge terms are very small compared to the dominant dipole contribution, which in itself is already insignificant because of the suppression by the j_2 function in the matrix element. There is thus no need to include these terms in the matrix element \mathcal{M}_2 for D -wave decay.

In the E1 approximation, the recoil factor M_f/M_i vanishes by eq. (6), since in that case $\vec{P}_f = \vec{P}_i$. The decay width expression (35) thus reduces to

$$\Gamma_{\text{E1}} = \mathcal{S}_{fi} \frac{2J_f + 1}{27} 4 q_{\text{nr}}^3 \alpha | \lim_{q \rightarrow 0} \mathcal{M}_0 |^2, \quad (42)$$

in the E1 approximation, which is similar to the expression given in ref. [5]. Here the "recoilless" q -value is given by $q_{\text{nr}} = M_i - M_f$. Note that the OGE exchange charge contribution survives in the E1 approximation, whereas the contribution from the scalar confining interaction as well as the Darwin-Foldy terms are eliminated.

The expression for the width of a spin-flip M1 transition between S -wave heavy quarkonium states can be written in the form

$$\Gamma_{\text{M1}} = \frac{16}{2S_i + 1} q^3 \alpha \frac{M_f}{M_i} |\mathcal{M}_\gamma|^2, \quad (43)$$

where \mathcal{M}_γ denotes the radial matrix element for M1 decay and S_i is the total spin of the initial state. The radial matrix element for M1 decay consists of relativistic impulse approximation, scalar confining and OGE components, according to

$$\mathcal{M}_\gamma = \mathcal{M}_\gamma^{\text{RIA}} + \mathcal{M}_\gamma^{\text{Conf}} + \mathcal{M}_\gamma^{\text{Oge}}, \quad (44)$$

where the different matrix elements can be obtained from the corresponding spin-flip magnetic moment operators by dropping the charge e and the spinors $\vec{\sigma}_1 - \vec{\sigma}_2$. From the relativistic matrix element (18) and the relativistic spin-flip magnetic moment operator (20), one obtains

$$\mathcal{M}_\gamma^{\text{RIA}} = \frac{2}{\pi} \int_0^\infty dr' r' u_f(r') \int_0^\infty dr r u_i(r) \int_0^\infty dP P^2 \frac{1}{4} \left[\frac{Q_1}{m_1} f_1^\gamma - \frac{Q_2}{m_2} f_2^\gamma \right] j_0(r'P) j_0(rP), \quad (45)$$

where the factors f_i^γ are given by eq. (20). The matrix elements associated with the scalar confining and vector OGE interactions are of the form

$$\mathcal{M}_\gamma^{\text{Conf}} = - \int_0^\infty dr u_f(r) u_i(r) \frac{V_c(r)}{4} \left[\frac{Q_1}{m_1^2} - \frac{Q_2}{m_2^2} \right], \quad (46)$$

for the scalar confining interaction, and

$$\mathcal{M}_\gamma^{\text{Oge}} = - \int_0^\infty dr u_f(r) u_i(r) \frac{V_g(r)}{8} \left[\frac{Q_1}{m_1^2} - \frac{Q_2}{m_2^2} - \frac{Q_1 - Q_2}{m_1 m_2} \right], \quad (47)$$

for the OGE interaction.

It should be noted at this point that the appearance of two-quark matrix elements as given above is entirely due to the elimination in the impulse approximation of the negative energy components in the reduction of the Bethe-Salpeter equation to a Blankenbecler-Sugar equation. These components do however contribute as transition matrix elements, and have to be included in the Blankenbecler-Sugar (or Schrödinger) framework as explicit two-quark current operators [19], as illustrated in Fig. 1. In e.g. the alternate Gross type reduction of the Bethe-Salpeter equation, these two-quark operators are automatically taken into account by the single quark transition operators.

3.3 Magnetic moment of the B_c^\pm

Of the heavy quarkonium systems, only the spin-triplet B_c^\pm ($c\bar{b}$, $\bar{c}b$) states have a magnetic moment. That may be calculated from the spin-symmetric part of eq. (19). When expressed in terms of the nuclear magneton μ_N , the magnetic moment of the B_c^{*+} ($c\bar{b}$) state is obtained as

$$\mu_{c\bar{b}} = \frac{m_p}{3} \left[\frac{2}{m_c} + \frac{1}{m_b} \right] \mu_N, \quad (48)$$

where m_p is the proton mass. The above expression is valid in the nonrelativistic limit. Since it is known that the magnetic moments of the baryons receive significant corrections from relativistic effects [23], then a relativistic version of eq. (48) is called for. In the relativistic impulse approximation, the magnetic moment of an S -wave $c\bar{b}$ state is of the form

$$\mu_{c\bar{b}}^{\text{RIA}} = \frac{2}{\pi} \int_0^\infty dr dr' r r' u(r) u(r') \int_0^\infty dP P^2 \frac{m_p}{3} \left[\frac{2}{m_c} f_c^\gamma + \frac{1}{m_b} f_b^\gamma \right] j_0(r'P) j_0(rP) \mu_N, \quad (49)$$

where $u(r)$ is the reduced radial wavefunction of the $c\bar{b}$ state. In eq. (49), the factors f_i^γ are defined in eq. (20). In addition to the relativistic impulse approximation, the exchange magnetic moment operators associated with the scalar confining and vector OGE interactions will also contribute to the magnetic moment of the B_c^\pm . The contribution from the scalar confining interaction is of the form

$$\mu_{c\bar{b}}^{\text{Conf}} = - \int_0^\infty dr u^2(r) V_c(r) \frac{m_p}{3} \left[\frac{2}{m_c^2} + \frac{1}{m_b^2} \right] \mu_N, \quad (50)$$

where the confining interaction $V_c(r)$ is of the form $V_c(r) = cr$. Similarly, the OGE contribution can be expressed as

$$\mu_{c\bar{b}}^{\text{Oge}} = - \int_0^\infty dr u^2(r) V_g(r) \frac{m_p}{6} \left[\frac{2}{m_c^2} + \frac{1}{m_b^2} + \frac{3}{m_c m_b} \right] \mu_N, \quad (51)$$

where the OGE potential $V_g(r)$ is given by the Fourier transform of eq. (31). The total magnetic moment of the $B_c^{*\pm}$ is thus given by the sum of the RIA contribution (49) and the exchange contributions (50) and (51).

4 Numerical Results

This section presents the numerical values of the widths and matrix elements for each E1 and M1 transition, as obtained using the model for the $Q\bar{Q}$ spectra presented in section 3.1. Unless otherwise indicated, the E1 widths have been calculated using eqs. (35), (36), (37) and (38), while the widths for M1 decay correspond to eqs. (43) and (44). When the mass of one of the quarkonium states is not known empirically, then the splittings rather than the absolute values from Table 1 are used to determine the photon momentum q_γ .

The widths for M1 transitions between S -wave states in charmonium and bottomonium are given in Table 3, along with the associated impulse approximation and exchange current matrix elements. For $c\bar{c}$ and $b\bar{b}$, the width for M1 decay is given by the sum of the impulse approximation and scalar confinement terms. In the case of the B_c^\pm , the widths for M1 decay also receive a contribution from the OGE exchange current. The M1 widths and magnetic moments of the B_c^\pm states are given in Tables 10 and 13, respectively. The widths of the E1 dominated transitions between low-lying $c\bar{c}$ and $b\bar{b}$ states are given in Tables 4, 5, 6, 7 and 8. They have been calculated both for the dynamical model presented in section 2.1 and the rigorous E1 approximation. The computed widths for E1 dominated transitions in the B_c^\pm system are given, along with the matrix elements, in Tables 9, 11 and 12.

Table 3: The M1 transitions between low-lying S -wave states in the charmonium ($c\bar{c}$) and bottomonium ($b\bar{b}$) systems. Experimental data [10] is available only for the $J/\psi \rightarrow \eta_c\gamma$ and $\psi' \rightarrow \eta_c\gamma$ transitions. Note that the empirical value for $\psi' \rightarrow \eta_c\gamma$ is uncertain since the total width of the ψ' is poorly known. The quoted photon momenta q_γ have been obtained by combination of the empirical masses of the spin triplet states [10] with the splittings given by the Hamiltonian model of ref. [15] in Table 1. The M1 decays of the $\psi(3S)$ state have not been included since the $3S$ states in charmonium lie above the threshold for $D\bar{D}$ fragmentation.

Transition	Matrix element [fm]			Width		
	NRIA	RIA	Conf	NRIA	RIA	RIA+Conf
$J/\psi \rightarrow \eta_c\gamma$ $q_\gamma : 116 \text{ MeV}$	$4.356 \cdot 10^{-2}$	$3.762 \cdot 10^{-2}$	$-8.724 \cdot 10^{-3}$	2.85	2.12	1.25 keV exp: 1.14 ± 0.39
$\psi' \rightarrow \eta_c\gamma$ $q_\gamma : 639 \text{ MeV}$	$3.985 \cdot 10^{-3}$	$-5.14 \cdot 10^{-4}$	$2.826 \cdot 10^{-3}$	3.35	0.06	1.13 keV exp: 0.84 ± 0.24
$\psi' \rightarrow \eta'_c\gamma$ $q_\gamma : 46 \text{ MeV}$	$4.344 \cdot 10^{-2}$	$3.735 \cdot 10^{-2}$	$-1.870 \cdot 10^{-2}$	0.18	0.13	0.03 keV
$\eta'_c \rightarrow J/\psi\gamma$ $q_\gamma : 502 \text{ MeV}$	$-4.271 \cdot 10^{-3}$	$-7.584 \cdot 10^{-3}$	$5.206 \cdot 10^{-3}$	5.89	18.6	1.83 keV
<hr/>						
$\Upsilon \rightarrow \eta_b\gamma$ $q_\gamma : 59 \text{ MeV}$	$-6.71 \cdot 10^{-3}$	$-6.39 \cdot 10^{-3}$	$2.41 \cdot 10^{-4}$	9.2	8.3	7.7 eV
$\Upsilon(2S) \rightarrow \eta_b\gamma$ $q_\gamma : 603 \text{ MeV}$	$-3.94 \cdot 10^{-4}$	$-1.44 \cdot 10^{-4}$	$-8.76 \cdot 10^{-5}$	31.8	4.3	11.0 eV
$\Upsilon(2S) \rightarrow \eta_b(2S)\gamma$ $q_\gamma : 25 \text{ MeV}$	$-6.70 \cdot 10^{-3}$	$-6.39 \cdot 10^{-3}$	$5.45 \cdot 10^{-4}$	0.70	0.64	0.53 eV
$\eta_b(2S) \rightarrow \Upsilon\gamma$ $q_\gamma : 530 \text{ MeV}$	$4.18 \cdot 10^{-4}$	$6.30 \cdot 10^{-4}$	$-1.31 \cdot 10^{-4}$	71.5	162	102 eV
$\Upsilon(3S) \rightarrow \eta_b(3S)\gamma$ $q_\gamma : 16 \text{ MeV}$	$-6.70 \cdot 10^{-3}$	$-6.35 \cdot 10^{-3}$	$8.02 \cdot 10^{-4}$	0.18	0.16	0.13 eV
$\Upsilon(3S) \rightarrow \eta_b(2S)\gamma$ $q_\gamma : 350 \text{ MeV}$	$-3.59 \cdot 10^{-4}$	$-1.11 \cdot 10^{-4}$	$-1.55 \cdot 10^{-4}$	5.3	0.5	2.9 eV
$\Upsilon(3S) \rightarrow \eta_b\gamma$ $q_\gamma : 910 \text{ MeV}$	$-2.10 \cdot 10^{-4}$	$-6.59 \cdot 10^{-5}$	$-3.77 \cdot 10^{-5}$	30.2	3.0	7.3 eV
$\eta_b(3S) \rightarrow \Upsilon(2S)\gamma$ $q_\gamma : 311 \text{ MeV}$	$3.96 \cdot 10^{-4}$	$6.05 \cdot 10^{-4}$	$-2.25 \cdot 10^{-4}$	13.7	32.0	12.6 eV
$\eta_b(3S) \rightarrow \Upsilon\gamma$ $q_\gamma : 842 \text{ MeV}$	$2.05 \cdot 10^{-4}$	$3.02 \cdot 10^{-4}$	$-4.68 \cdot 10^{-5}$	68.7	149	106 eV

Table 4: The E1 dominated transitions between low-lying states in the charmonium ($c\bar{c}$) system, together with the empirical data given by ref. [11]. The column "IA" contains the matrix element (37) in the impulse (single quark) approximation, while in the column labeled "DYN", the exchange charge contributions have been included. The columns "E1" contain the matrix element and the γ width in the E1 approximation. The q_γ values, as given above, have been rounded to the nearest MeV, and correspond wherever possible to the empirical data in Table 1. Further E1 transitions can be found in Table 8.

Transition	\mathcal{M}_0 [fm]			\mathcal{M}_2 [fm]	Width	
	IA	DYN	E1		E1	DYN
$\chi_{c2} \rightarrow J/\psi \gamma$ $q_\gamma : 429$ MeV	0.2389	0.2442	0.2632	$7.145 \cdot 10^{-3}$	558 keV	343 keV exp: 389 ± 60
$\chi_{c1} \rightarrow J/\psi \gamma$ $q_\gamma : 390$ MeV	0.2464	0.2519	0.2673	$5.729 \cdot 10^{-3}$	422 keV	276 keV exp: 290 ± 60
$\chi_{c0} \rightarrow J/\psi \gamma$ $q_\gamma : 303$ MeV	0.2556	0.2612	0.2701	$3.345 \cdot 10^{-3}$	196 keV	144 keV exp: 165 ± 40
$\psi' \rightarrow \chi_{c0} \gamma$ $q_\gamma : 261$ MeV	-0.2685	-0.2686	-0.2840	$-6.106 \cdot 10^{-3}$	44.6 keV	33.1 keV exp: 26.1 ± 4.5
$\psi' \rightarrow \chi_{c1} \gamma$ $q_\gamma : 171$ MeV	-0.3126	-0.3126	-0.3202	$-3.028 \cdot 10^{-3}$	45.8 keV	38.7 keV exp: 25.2 ± 4.5
$\psi' \rightarrow \chi_{c2} \gamma$ $q_\gamma : 127$ MeV	-0.3440	-0.3442	-0.3489	$-1.871 \cdot 10^{-3}$	37.1 keV	33.1 keV exp: 20.4 ± 4.0
$h_c \rightarrow \eta_c \gamma$ $q_\gamma : 493$ MeV $\mathcal{S}_{fi} : 3$	0.2098	0.2091	0.2289	$7.377 \cdot 10^{-3}$	661 keV	370 keV
$\eta'_c \rightarrow h_c \gamma$ $q_\gamma : 125$ MeV $\mathcal{S}_{fi} : 3$	-0.3420	-0.3424	-0.3465	$-1.618 \cdot 10^{-3}$	61.5 keV	55.0 keV
$\psi(3S) \rightarrow \chi_{c0} \gamma$ $q_\gamma : 577$ MeV	-0.0456	-0.0450	-0.0199	$0.926 \cdot 10^{-2}$	2.69 keV	9.86 keV
$\psi(3S) \rightarrow \chi_{c1} \gamma$ $q_\gamma : 494$ MeV	-0.0306	-0.0298	-0.0033	$1.016 \cdot 10^{-2}$	0.13 keV	9.57 keV
$\psi(3S) \rightarrow \chi_{c2} \gamma$ $q_\gamma : 455$ MeV	-0.0168	-0.0161	0.0123	$1.099 \cdot 10^{-2}$	2.38 keV	5.75 keV
$\psi(3S) \rightarrow \chi_{c0}(2P) \gamma$ $q_\gamma : 153$ MeV	-0.4315	-0.4315	-0.4497	$-7.344 \cdot 10^{-3}$	21.3 keV	17.8 keV
$\psi(3S) \rightarrow \chi_{c1}(2P) \gamma$ $q_\gamma : 125$ MeV	-0.4860	-0.4861	-0.4995	$-5.399 \cdot 10^{-3}$	42.6 keV	37.3 keV
$\psi(3S) \rightarrow \chi_{c2}(2P) \gamma$ $q_\gamma : 109$ MeV	-0.5280	-0.5283	-0.5391	$-4.367 \cdot 10^{-3}$	53.7 keV	48.2 keV

Table 5: The E1 dominated transitions between low-lying states in the bottomonium ($b\bar{b}$) system, together with the empirical data given by ref. [10]. The column "IA" contains the matrix element (37) in the impulse (single quark) approximation, while in the column labeled "DYN", the exchange charge contributions have been included. The columns "E1" contain the matrix element and the γ width in the E1 approximation. The photon momenta q_γ have been obtained as for Table 4. Further E1 transitions that involve the $\chi_{bJ}(2P)$ states can be found in Table 8.

Transition	\mathcal{M}_0 [fm]			\mathcal{M}_2 [fm]		Width	
	IA	DYN	E1	E1	E1	E1	DYN
$\chi_{b2} \rightarrow \Upsilon \gamma$ $q_\gamma : 443$ MeV	-0.0721	-0.0723	-0.0743	$-7.76 \cdot 10^{-4}$	42.7 keV	36.0 keV	Br: $22 \pm 3\%$
$\chi_{b1} \rightarrow \Upsilon \gamma$ $q_\gamma : 424$ MeV	-0.0731	-0.0733	-0.0751	$-6.96 \cdot 10^{-4}$	38.1 keV	32.5 keV	Br: $35 \pm 8\%$
$\chi_{b0} \rightarrow \Upsilon \gamma$ $q_\gamma : 392$ MeV	-0.0742	-0.0743	-0.0759	$-5.80 \cdot 10^{-4}$	30.7 keV	26.6 keV	Br: $< 6\%$
$\Upsilon(2S) \rightarrow \chi_{b0} \gamma$ $q_\gamma : 162$ MeV	0.0935	0.0935	0.0942	$2.90 \cdot 10^{-4}$	1.07 keV	1.01 keV	exp: 1.7 ± 0.5
$\Upsilon(2S) \rightarrow \chi_{b1} \gamma$ $q_\gamma : 129$ MeV	0.1007	0.1007	0.1012	$2.01 \cdot 10^{-4}$	1.88 keV	1.80 keV	exp: 3.0 ± 0.7
$\Upsilon(2S) \rightarrow \chi_{b2} \gamma$ $q_\gamma : 109$ MeV	0.1063	0.1063	0.1067	$1.53 \cdot 10^{-4}$	2.10 keV	2.03 keV	exp: 3.1 ± 0.7
$h_b \rightarrow \eta_b \gamma$ $q_\gamma : 485$ MeV $S_{fi} : 3$	-0.0664	-0.0664	-0.0685	$-7.98 \cdot 10^{-4}$	47.9 keV	39.7 keV	
$\eta_b(2S) \rightarrow h_b \gamma$ $q_\gamma : 100$ MeV $S_{fi} : 3$	0.1066	0.1066	0.1069	$1.20 \cdot 10^{-4}$	2.86 keV	2.77 keV	
$\Upsilon(3S) \rightarrow \chi_{b0} \gamma$ $q_\gamma : 483$ MeV	0.0068	0.0068	0.0039	$-1.13 \cdot 10^{-3}$	0.05 keV	0.15 keV	
$\Upsilon(3S) \rightarrow \chi_{b1} \gamma$ $q_\gamma : 452$ MeV	0.0036	0.0036	0.0005	$-1.20 \cdot 10^{-3}$	2.2 eV	0.11 keV	
$\Upsilon(3S) \rightarrow \chi_{b2} \gamma$ $q_\gamma : 433$ MeV	0.0007	0.0007	-0.0025	$-1.26 \cdot 10^{-3}$	0.08 keV	0.04 keV	
$\Upsilon(3S) \rightarrow \chi_{b0}(2P) \gamma$ $q_\gamma : 122$ MeV	0.1505	0.1504	0.1520	$6.18 \cdot 10^{-4}$	1.19 keV	1.14 keV	exp: 1.4 ± 0.3
$\Upsilon(3S) \rightarrow \chi_{b1}(2P) \gamma$ $q_\gamma : 100$ MeV	0.1614	0.1613	0.1624	$4.36 \cdot 10^{-4}$	2.20 keV	2.12 keV	exp: 3.0 ± 0.5
$\Upsilon(3S) \rightarrow \chi_{b2}(2P) \gamma$ $q_\gamma : 86$ MeV	0.1699	0.1699	0.1707	$3.38 \cdot 10^{-4}$	2.57 keV	2.50 keV	exp: 3.0 ± 0.6

Table 6: The E1 transitions from the lightest spin-triplet D -wave states in charmonium ($c\bar{c}$). The labeling of the columns is as for Tables 4 and 5, and the photon momenta q_γ have been calculated from the D -wave masses predicted in Table 1. The statistical factors \mathcal{S}_{fi} are given by eq. (36). Note that a good experimental candidate [10] for the 3D_1 state is the $\psi(3770)$ resonance.

Transition	\mathcal{M}_0 [fm]			Width	
	IA	DYN	E1	E1	DYN
${}^3D_3 \rightarrow \chi_{c2} \gamma$ $q_\gamma : 227 \text{ MeV } \mathcal{S}_{fi} : 18/25$	0.4164	0.4194	0.4353	243 keV	192 keV
${}^3D_2 \rightarrow \chi_{c2} \gamma$ $q_\gamma : 221 \text{ MeV } \mathcal{S}_{fi} : 9/50$	0.4188	0.4219	0.4367	56.5 keV	45.2 keV
${}^3D_2 \rightarrow \chi_{c1} \gamma$ $q_\gamma : 263 \text{ MeV } \mathcal{S}_{fi} : 9/10$	0.3920	0.3953	0.4145	262 keV	198 keV
${}^3D_1 \rightarrow \chi_{c2} \gamma$ $q_\gamma : 206 \text{ MeV } \mathcal{S}_{fi} : 1/50$	0.4216	0.4246	0.4372	5.06 keV	4.13 keV
${}^3D_1 \rightarrow \chi_{c1} \gamma$ $q_\gamma : 248 \text{ MeV } \mathcal{S}_{fi} : 1/2$	0.3963	0.3997	0.4164	123 keV	94.9 keV
${}^3D_1 \rightarrow \chi_{c0} \gamma$ $q_\gamma : 336 \text{ MeV } \mathcal{S}_{fi} : 2$	0.3578	0.3619	0.3889	370 keV	251 keV

Table 7: The E1 transitions from the lightest spin-triplet D -wave states in bottomonium ($b\bar{b}$). The photon momenta q_γ and statistical factors \mathcal{S}_{fi} have been calculated as for Table 6.

Transition	\mathcal{M}_0 [fm]			Width	
	IA	DYN	E1	E1	DYN
${}^3D_3 \rightarrow \chi_{b2} \gamma$ $q_\gamma : 242 \text{ MeV } \mathcal{S}_{fi} : 18/25$	-0.1270	-0.1271	-0.1291	24.5 keV	22.3 keV
${}^3D_2 \rightarrow \chi_{b2} \gamma$ $q_\gamma : 233 \text{ MeV } \mathcal{S}_{fi} : 9/50$	-0.1275	-0.1276	-0.1295	5.51 keV	5.04 keV
${}^3D_2 \rightarrow \chi_{b1} \gamma$ $q_\gamma : 253 \text{ MeV } \mathcal{S}_{fi} : 9/10$	-0.1228	-0.1229	-0.1250	19.6 keV	17.8 keV
${}^3D_1 \rightarrow \chi_{b2} \gamma$ $q_\gamma : 223 \text{ MeV } \mathcal{S}_{fi} : 1/50$	-0.1280	-0.1280	-0.1297	0.54 keV	0.50 keV
${}^3D_1 \rightarrow \chi_{b1} \gamma$ $q_\gamma : 243 \text{ MeV } \mathcal{S}_{fi} : 1/2$	-0.1234	-0.1235	-0.1254	9.75 keV	8.89 keV
${}^3D_1 \rightarrow \chi_{b0} \gamma$ $q_\gamma : 275 \text{ MeV } \mathcal{S}_{fi} : 2$	-0.1173	-0.1174	-0.1196	17.3 keV	15.5 keV

Table 8: The E1 transitions from the $2P$ states in charmonium ($c\bar{c}$) and bottomonium ($b\bar{b}$). The labeling of the states and the photon momenta q_γ for the transitions are as for Tables 4 and 5.

Transition	\mathcal{M}_0 [fm]			\mathcal{M}_2 [fm]	Width	
	IA	DYN	E1		E1	DYN
$\chi_{c2}(2P) \rightarrow \psi' \gamma$ $q_\gamma : 236$ MeV	0.3702	0.3735	0.4007	$1.09 \cdot 10^{-2}$	194 keV	144 keV
$\chi_{c1}(2P) \rightarrow \psi' \gamma$ $q_\gamma : 220$ MeV	0.3996	0.4031	0.4271	$9.60 \cdot 10^{-3}$	178 keV	137 keV
$\chi_{c0}(2P) \rightarrow \psi' \gamma$ $q_\gamma : 193$ MeV	0.4321	0.4357	0.4543	$7.43 \cdot 10^{-3}$	133 keV	108 keV
$\chi_{c2}(2P) \rightarrow J/\psi \gamma$ $q_\gamma : 745$ MeV	0.0660	0.0693	0.0526	$-6.49 \cdot 10^{-3}$	133 keV	132 keV
$\chi_{c1}(2P) \rightarrow J/\psi \gamma$ $q_\gamma : 731$ MeV	0.0549	0.0581	0.0380	$-7.83 \cdot 10^{-3}$	65.3 keV	90.1 keV
$\chi_{c0}(2P) \rightarrow J/\psi \gamma$ $q_\gamma : 707$ MeV	0.0387	0.0417	0.0183	$-9.13 \cdot 10^{-3}$	13.6 keV	44.9 keV
$h_c(2P) \rightarrow \eta'_c \gamma$ $q_\gamma : 263$ MeV $\mathcal{S}_{fi} : 3$	0.3444	0.3450	0.3752	$1.21 \cdot 10^{-2}$	236 keV	167 keV
$h_c(2P) \rightarrow \eta_c \gamma$ $q_\gamma : 821$ MeV $\mathcal{S}_{fi} : 3$	0.0646	0.0631	0.0489	$-5.44 \cdot 10^{-3}$	161 keV	142 keV
$\chi_{b2}(2P) \rightarrow \Upsilon(2S) \gamma$ $q_\gamma : 243$ MeV	-0.1186	-0.1186	-0.1221	$-1.38 \cdot 10^{-3}$	18.5 keV	16.4 keV
					Br: 16.2 ± 2.4 %	
$\chi_{b1}(2P) \rightarrow \Upsilon(2S) \gamma$ $q_\gamma : 229$ MeV	-0.1240	-0.1241	-0.1272	$-1.23 \cdot 10^{-3}$	16.8 keV	15.1 keV
					Br: 21 ± 4 %	
$\chi_{b0}(2P) \rightarrow \Upsilon(2S) \gamma$ $q_\gamma : 207$ MeV	-0.1305	-0.1306	-0.1331	$-1.01 \cdot 10^{-3}$	13.5 keV	12.3 keV
					Br: 4.6 ± 2.1 %	
$\chi_{b2}(2P) \rightarrow \Upsilon \gamma$ $q_\gamma : 777$ MeV	-0.0176	-0.0177	-0.0156	$8.44 \cdot 10^{-4}$	10.7 keV	11.4 keV
					Br: 7.1 ± 1.0 %	
$\chi_{b1}(2P) \rightarrow \Upsilon \gamma$ $q_\gamma : 764$ MeV	-0.0155	-0.0156	-0.0132	$9.28 \cdot 10^{-4}$	7.32 keV	8.40 keV
					Br: 8.5 ± 1.3 %	
$\chi_{b0}(2P) \rightarrow \Upsilon \gamma$ $q_\gamma : 743$ MeV	-0.0123	-0.0124	-0.0098	$1.01 \cdot 10^{-3}$	3.70 keV	4.93 keV
					Br: 0.9 ± 0.6 %	
$h_b(2P) \rightarrow \eta_b(2S) \gamma$ $q_\gamma : 257$ MeV $\mathcal{S}_{fi} : 3$	-0.1120	-0.1120	-0.1155	$-1.42 \cdot 10^{-3}$	19.5 keV	17.2 keV
$h_b(2P) \rightarrow \eta_b \gamma$ $q_\gamma : 821$ MeV $\mathcal{S}_{fi} : 3$	-0.0179	-0.0179	-0.0160	$7.43 \cdot 10^{-3}$	13.4 keV	13.5 keV

Table 9: The E1 dominated transitons between low-lying states in the $B_c^\pm (c\bar{b})$ system. The labeling of the columns is as for Tables 4 and 5. Note that spin-triplet states are indicated by "stars" in their labels. The q_γ values have been obtained as for Table 4. Further E1 transitions can be found in Table 11.

Transition	\mathcal{M}_0 [fm]			\mathcal{M}_2 [fm]	Width	
	IA	DYN	E1		E1	DYN
$B_{c2}^* \rightarrow B_c^* \gamma$ $q_\gamma : 397$ MeV	0.1361	0.1386	0.1453	$2.43 \cdot 10^{-3}$	120 keV	93.9 keV
$B_{c1}^* \rightarrow B_c^* \gamma$ $q_\gamma : 379$ MeV	0.1382	0.1408	0.1469	$2.16 \cdot 10^{-3}$	107 keV	84.6 keV
$B_{c0}^* \rightarrow B_c^* \gamma$ $q_\gamma : 352$ MeV	0.1403	0.1429	0.1480	$1.81 \cdot 10^{-3}$	86.6 keV	70.4 keV
$B_c^*(2S) \rightarrow B_{c0}^* \gamma$ $q_\gamma : 184$ MeV	-0.1578	-0.1578	-0.1610	$-1.28 \cdot 10^{-3}$	4.71 keV	4.22 keV
$B_c^*(2S) \rightarrow B_{c1}^* \gamma$ $q_\gamma : 157$ MeV	-0.1720	-0.1720	-0.1746	$-1.01 \cdot 10^{-3}$	10.2 keV	9.35 keV
$B_c^*(2S) \rightarrow B_{c2}^* \gamma$ $q_\gamma : 139$ MeV	-0.1842	-0.1843	-0.1864	$-0.85 \cdot 10^{-3}$	13.2 keV	12.3 keV
$B_{c1} \rightarrow B_c \gamma$ $q_\gamma : 431$ MeV $S_{fi} : 3$	0.1267	0.1283	0.1353	$2.50 \cdot 10^{-3}$	135 keV	103 keV
$B_c(2S) \rightarrow B_{c1} \gamma$ $q_\gamma : 133$ MeV $S_{fi} : 3$	-0.1834	-0.1835	-0.1854	$-0.73 \cdot 10^{-3}$	20.7 keV	19.3 keV

Table 10: The M1 transitions between low-lying S -wave states in the $B_c^\pm (c\bar{b})$ system. The matrix elements of the spin-flip operator associated with the OGE interaction are given in the column labeled "Oge". The $3S$ states have not been considered as they lie above the BD fragmentation threshold.

Transition	Matrix element [10^{-3} fm]				Width		
	NRIA	RIA	Conf	Oge	NRIA	RIA	RIA+Exch
$B_c^* \rightarrow B_c \gamma$ $q_\gamma : 53$ MeV	18.51	14.96	-3.643	3.969	50.0 eV	32.6 eV	34.0 eV
$B_c^*(2S) \rightarrow B_c \gamma$ $q_\gamma : 576$ MeV	1.015	-1.437	1.342	1.182	179 eV	360 eV	206 eV
$B_c^*(2S) \rightarrow B_c(2S) \gamma$ $q_\gamma : 22$ MeV	18.49	14.80	-7.666	2.480	3.61 eV	2.31 eV	0.98 eV
$B_c(2S) \rightarrow B_c^* \gamma$ $q_\gamma : 507$ MeV	-1.067	-3.089	1.924	8.351	411 eV	3.44 keV	39.5 eV

Table 11: The E1 transitions from the $2P$ states in the B_c^\pm ($c\bar{b}$) system. The labeling of the states and the photon momenta q_γ for the transitions are as for Tables 4 and 5.

Transition	\mathcal{M}_0 [fm]			\mathcal{M}_2 [fm]	Width	
	IA	DYN	E1		E1	DYN
$B_{c2}^*(2P) \rightarrow B_c^*(2S) \gamma$ $q_\gamma : 222$ MeV	0.2151	0.2166	0.2265	$3.94 \cdot 10^{-3}$	49.3 keV	41.7 keV
$B_{c1}^*(2P) \rightarrow B_c^*(2S) \gamma$ $q_\gamma : 212$ MeV	0.2263	0.2279	0.2370	$3.59 \cdot 10^{-3}$	46.5 keV	39.9 keV
$B_{c0}^*(2P) \rightarrow B_c^*(2S) \gamma$ $q_\gamma : 194$ MeV	0.2381	0.2398	0.2474	$3.04 \cdot 10^{-3}$	39.0 keV	34.2 keV
$B_{c2}^*(2P) \rightarrow B_c^* \gamma$ $q_\gamma : 733$ MeV	0.0320	0.0333	0.0264	$-2.97 \cdot 10^{-3}$	27.0 keV	32.9 keV
$B_{c1}^*(2P) \rightarrow B_c^* \gamma$ $q_\gamma : 723$ MeV	0.0270	0.0283	0.0204	$-3.34 \cdot 10^{-3}$	15.5 keV	23.2 keV
$B_{c0}^*(2P) \rightarrow B_c^* \gamma$ $q_\gamma : 707$ MeV	0.0207	0.0220	0.0131	$-3.69 \cdot 10^{-3}$	5.95 keV	13.4 keV
$B_{c1}(2P) \rightarrow B_c(2S) \gamma$ $q_\gamma : 234$ MeV $\mathcal{S}_{fi} : 3$	0.2065	0.2076	0.2179	$4.08 \cdot 10^{-3}$	53.3 keV	44.5 keV
$B_{c1}(2P) \rightarrow B_c \gamma$ $q_\gamma : 771$ MeV $\mathcal{S}_{fi} : 3$	0.0316	0.0323	0.0259	$-2.75 \cdot 10^{-3}$	30.6 keV	35.7 keV

Table 12: The E1 transitions from the lightest spin-triplet D -wave states in the B_c^\pm ($c\bar{b}$) system. The labeling of the states, the photon momenta q_γ and statistical factors \mathcal{S}_{fi} are as for Table 6.

Transition	\mathcal{M}_0 [fm]			Width	
	IA	DYN	E1	E1	DYN
$^3D_3 \rightarrow B_{c2}^* \gamma$ $q_\gamma : 235$ MeV $\mathcal{S}_{fi} : 18/25$	0.2270	0.2285	0.2352	75.7 keV	65.4 keV
$^3D_2 \rightarrow B_{c2}^* \gamma$ $q_\gamma : 232$ MeV $\mathcal{S}_{fi} : 9/50$	0.2279	0.2294	0.2358	18.3 keV	15.9 keV
$^3D_2 \rightarrow B_{c1}^* \gamma$ $q_\gamma : 250$ MeV $\mathcal{S}_{fi} : 9/10$	0.2181	0.2197	0.2267	63.9 keV	54.7 keV
$^3D_1 \rightarrow B_{c2}^* \gamma$ $q_\gamma : 224$ MeV $\mathcal{S}_{fi} : 1/50$	0.2288	0.2303	0.2362	1.84 keV	1.61 keV
$^3D_1 \rightarrow B_{c1}^* \gamma$ $q_\gamma : 243$ MeV $\mathcal{S}_{fi} : 1/2$	0.2193	0.2209	0.2274	32.5 keV	28.0 keV
$^3D_1 \rightarrow B_{c0}^* \gamma$ $q_\gamma : 270$ MeV $\mathcal{S}_{fi} : 2$	0.2079	0.2096	0.2170	54.4 keV	45.9 keV

	B_c^*	$B_c^*(2S)$	$B_c^*(3S)$
NRIA	$0.4810 \mu_N$	$0.4810 \mu_N$	$0.4810 \mu_N$
RIA	$0.4135 \mu_N$	$0.4075 \mu_N$	$0.3973 \mu_N$
Conf	$-0.0166 \mu_N$	$-0.0342 \mu_N$	$-0.0487 \mu_N$
Oge	$0.0292 \mu_N$	$0.0186 \mu_N$	$0.0146 \mu_N$
Total	$0.426 \mu_N$	$0.392 \mu_N$	$0.363 \mu_N$

Table 13: The magnetic moments of the S -wave $c\bar{b}$ states in units of nuclear magnetons. The RIA magnetic moment is given by eq. (49), and the exchange current contributions from the scalar confining and OGE interactions by eqs. (50) and (51), respectively. Note that the NRIA results are equivalent to those given by the static quark model.

5 Discussion

It is instructive to compare the numerical results of the previous section both with experiment and with those of other theoretical calculations, as there are several issues that are not readily apparent by casual inspection of the data presented in Tables 3 through 13. A direct comparison with the experimental averages given in ref. [10] may be misleading, as the branching fractions for various transitions are typically better known than the total width of the decaying state. Also, as recently published results [11] for $\chi_{cJ} \rightarrow J/\psi \gamma$ indicate that these E1 widths are significantly larger than previously thought [10], then a review of the model predictions is called for.

5.1 M1 transitions in the $c\bar{c}$ system

- $J/\psi \rightarrow \eta_c \gamma$

The observed width of 1.14 ± 0.39 keV for the M1 transition $J/\psi \rightarrow \eta_c \gamma$ has been difficult to explain theoretically [13], since previous calculations typically overestimate it by a factor ~ 3 . A possible solution for this overprediction, already hinted at in ref. [3], is presented in Table 3, where the exchange current contribution from the scalar confining interaction brings the width down to the desired level. However, as shown in ref. [14], expansion of the RIA spin-flip operator to order v^2/c^2 overestimates the correction to the static quark model result, and in that case the usefulness of the exchange current contribution is not apparent. The importance of negative energy components for the transition $J/\psi \rightarrow \eta_c \gamma$ has also been established within the instantaneous approximation to the Bethe-Salpeter equation in ref. [12] and the Schrödinger approach in ref. [14], where widths close to that given in Table 3 were obtained for a scalar confining interaction. If the whole $Q\bar{Q}$ potential had effective vector coupling structure, then no exchange current contribution would arise, as a vector interaction contributes a spin-flip operator only if the quark and antiquark masses are unequal, and agreement with experiment would thus be excluded. Other possible solutions include the introduction of a large anomalous magnetic moment for the charm quark [3], but this possibility has apparently not been substantiated.

- $\psi' \rightarrow \eta_c \gamma$

This nonrelativistically forbidden M1 transition has also proved theoretically challenging, since the (near) orthogonality of the quarkonium wavefunctions leads to model-dependent results. In the recent calculation by ref. [12], where good agreement with experiment was found for $J/\psi \rightarrow \eta_c \gamma$,

the width for $\psi' \rightarrow \eta_c \gamma$ was however overpredicted by almost an order of magnitude. The present calculation gives a width of ~ 1.1 keV for that transition, which is close to the empirical value 0.84 ± 0.24 keV [11]. This result is, however, not robust. That such a favorable result is obtained depends delicately on several factors, such as the employment of ψ' and η_c wavefunctions that include the spin-spin interaction in the S -wave, and the choice of approximation for the M1 matrix element.

The amplitude (15) has the advantage of allowing the use of a realistic photon momentum in the expression (43) for the M1 width. It is useful to note that this treatment yields the same spin-flip operators than had the rigorous M1 approximation been used, as in the calculation of the exchange magnetic moment operators in refs. [24, 22]. Furthermore, the M1 approximation has been taken to affect the entire factor in brackets in eq. (15). If the exponentials were separated from the current operators in eq. (15), then the width for $\psi' \rightarrow \eta_c \gamma$ would be overpredicted by a factor ~ 4 . However, if spin-averaged wavefunctions were employed, as in ref. [14], then the conclusion would be exactly the opposite; In that case the present treatment would lead to unfavorable results. As seen from Table 3, the exchange current operator associated with the scalar confining interaction gives the main contribution to the width for $\psi' \rightarrow \eta_c \gamma$ within this calculation. The present treatment of the M1 approximation may be regarded as consistent since it leads to the correct spin-flip operators and simultaneously allows the recoil of the η_c to be taken into account. Further modifications to the M1 width for $\psi' \rightarrow \eta_c \gamma$ may result from a relativistic treatment of the exchange current operator (23) and consideration of possible D -wave admixture in the ψ' state due to the OGE tensor interaction.

5.2 M1 transitions in the $b\bar{b}$ and $c\bar{b}$ systems

- $\Upsilon \rightarrow \eta_b \gamma$

A reasonable prediction for the width of the M1 transition $\Upsilon \rightarrow \eta_b \gamma$ can be obtained as soon as the mass of the η_b state is constrained by experiment, as the contributions from two-quark operators are suppressed by the large mass of the b quark. The uncertainty in the constituent mass (4885 MeV) of the b quark is also nowadays rather small [5, 18]. As realistic models of the spin-spin splittings for S -wave quarkonia give an η_b mass around 9400 MeV, then the width for $\Upsilon \rightarrow \eta_b \gamma$ is likely to be less than 10 eV, as given in Table 3. However, the reliability of such predictions cannot be tested until the η_b state is discovered empirically.

- $B_c^* \rightarrow B_c \gamma$

At this time, the photon momenta involved in calculations of M1 widths in the $c\bar{b}$ system have to be extracted from model calculations of the $c\bar{b}$ mass spectrum. As shown in ref. [5], the mass of the spin triplet B_c^* state is rather well constrained, and is expected to be about 6350 MeV. However, there is in general no such agreement for the magnitude of the $B_c^* - B_c$ splitting, which determines the photon momentum of the $B_c^* \rightarrow B_c \gamma$ transition. Realistic models for the spin-spin interaction in the S -wave appear to favor a small splitting of ~ 40 MeV. In spite of this, the computed width for $B_c^* \rightarrow B_c \gamma$ of 34 eV given in Table 10 compares well with the ~ 29 eV predicted by ref. [5], even though exchange current contributions were not considered in that work. It is noteworthy that the exchange current contribution from the OGE interaction is dominant for $c\bar{b}$ and leads to a slight increase of the width for $B_c^* \rightarrow B_c \gamma$. Because of this cancellation, the nonrelativistic width is quite close to the net result.

Predictions have also been given, in Tables 3 and 10, for M1 transitions between $Q\bar{Q}$ states that lie below the respective fragmentation thresholds. Notable among these is $\psi' \rightarrow \eta'_c \gamma$, which is similar to $J/\psi \rightarrow \eta_c \gamma$. However, the suppression due to the scalar confining interaction is stronger as the $2S$ wavefunctions have a longer range. Also, as recent experimental results indicate that the mass of the η'_c is larger than previously thought [27], then the phase space available for $\psi' \rightarrow \eta'_c \gamma$ is also suppressed. Consequently the predicted width is also smaller than the values suggested by previous work [12]. As for the transition $\psi' \rightarrow \eta_c \gamma$, the width for $\eta'_c \rightarrow J/\psi \gamma$ is also sensitive to the particulars of the model because of cancellations in the matrix element and the large photon momentum. The results in Table 3 suggest that the width for this transition should be around 2 keV. As the experimental situation concerning the η'_c continues to improve, then the width for $\eta'_c \rightarrow J/\psi \gamma$ may possibly be measured in the near future.

In the case of the $b\bar{b}$ system, the number of measurable M1 transitions is larger since the $3S$ states of bottomonium lie below the threshold for $B\bar{B}$ fragmentation. The results of Table 3 indicate that most M1 transitions in the $b\bar{b}$ system are difficult to calculate accurately, and therefore provide an instructive test for model predictions. In particular, the widths for transitions that do not change the principal quantum number of the quarkonium state are predicted to be highly suppressed, whereas the widths for transitions from excited η_b states to the Υ ground state are predicted to have larger widths of about 100 eV.

5.3 E1 transitions in the $c\bar{c}$ system

While the M1 transitions in heavy quarkonia are sensitive to the Lorentz structure of the $Q\bar{Q}$ interaction, the E1 transitions have been shown here to receive only small contributions from the exchange current operators of Fig. 1. They typically increase the value of the matrix element so that its value in the dynamical model is between those in the impulse and E1 approximations. On the other hand, the matrix element of the dipole operator is sensitive to the shape of the $Q\bar{Q}$ wavefunctions, and thus a realistic description of the E1 widths requires that the hyperfine components of the $Q\bar{Q}$ interaction are not treated as first order perturbations. This conclusion is in line with that reached in ref. [18], which employed the nonsingular $Q\bar{Q}$ potential model of ref. [32]. Comparisons between the present results, those of previous calculations and experiment are given for several E1 transitions in $c\bar{c}$ and $b\bar{b}$ in Tables 14 and 15.

Table 14: Comparison of the results for E1 transitions in the charmonium ($c\bar{c}$) system with the predictions of other models, for a scalar confining interaction. All widths are given in keV. The experimental widths have been extracted from ref. [11].

	MB (ref. [1])	GS (ref. [3, 33])	MR (ref. [2])	This Work	Exp (ref. [11])
$\chi_{c2} \rightarrow J/\psi \gamma$	347	413	609	343	389 ± 60 keV
$\chi_{c1} \rightarrow J/\psi \gamma$	270	340	460	276	290 ± 60 keV
$\chi_{c0} \rightarrow J/\psi \gamma$	128	162	225	144	165 ± 40 keV
$\psi' \rightarrow \chi_{c2} \gamma$	27	26	41	33	20.4 ± 4.0 keV
$\psi' \rightarrow \chi_{c1} \gamma$	31	28	48	39	25.2 ± 4.5 keV
$\psi' \rightarrow \chi_{c0} \gamma$	19	18	37	33	26.1 ± 4.5 keV
$h_c \rightarrow \eta_c \gamma$	483	630	—	370	—

- $\chi_{cJ} \rightarrow J/\psi \gamma$

Predictions for the E1 transitions from the spin-triplet P -wave states in charmonium should be robust, as the quarkonium wavefunctions involved do not contain any nodes. The systematic overprediction of these widths by $\sim 20\%$, as indicated by the empirical data of ref. [10], has therefore been puzzling. However, in view of the most recent experimental data [11], this issue is apparently resolved. As seen from Table 14, models which consider the recoil of the J/ψ reproduce the empirical results remarkably well. In contrast, the rigorous E1 approximation leads to overpredictions of $\sim 50\%$.

- $\psi' \rightarrow \chi_{cJ} \gamma$

The E1 transitions from the ψ' state have, in general, been difficult to predict, since the E1 approximation has typically overestimated the empirical widths by at least a factor ~ 2 . The latest experimental data for the branching fractions for γ decay and total width of the ψ' suggests that the widths for $\psi' \rightarrow \chi_{cJ} \gamma$ should be around 25 keV, while the E1 approximation typically yields widths in excess of 40 keV. The results for $\psi' \rightarrow \chi_{cJ} \gamma$ obtained by ref. [12] within the framework of the instantaneous approximation to the Bethe-Salpeter equation, are also of the order ~ 40 keV. Recoil effects cannot account for this overprediction, as they are much weaker than for the $\chi_{cJ} \rightarrow J/\psi \gamma$ transitions. However, inspection of Table 14 reveals that the predicted relative widths are also not in agreement with experiment, although the uncertainties are considerable. This suggests a sensitivity to small changes in the $Q\bar{Q}$ wavefunctions, which is indeed revealed by inspection of the matrix elements in Table 4. The present empirical data suggests that the width for $\psi' \rightarrow \chi_{c2} \gamma$ should be the smallest. Of the models presented in Table 14, the present one comes closest to this result. It should also be noted that significant reductions of the E1 widths have been obtained in ref. [34] by consideration of closed $c\bar{q} - q\bar{c}$ fragmentation channels.

The predicted widths for E1 transitions from the $\psi(3S)$ state have also been given in Table 4. The results suggest that the widths for transitions to the $2P$ states should be comparable to those for the $\psi' \rightarrow \chi_{cJ} \gamma$ transitions. On the other hand, the widths for the $\psi(3S) \rightarrow \chi_{cJ} \gamma$ transitions are predicted to be smaller by a factor ~ 4 . The empirical detection of any of these transitions will probably be challenging since the $\psi(3S)$ state decays mainly through $D\bar{D}$ fragmentation. However, the photon produced in the $h_c \rightarrow \eta_c \gamma$ transition will probably be detected in the near future, as that state lies well below the $D\bar{D}$ fragmentation threshold. The results presented in Table 14 suggest that the E1 width for that transition is the largest in the $c\bar{c}$ system. However, the uncertainty in that prediction is somewhat larger because of recoil effects and the hitherto uncertain mass of the h_c state. Of particular interest are also the E1 transitions from the 3D_1 state given in Table 6, as that state probably corresponds to the empirical $\psi(3770)$ resonance. The calculated widths suggest that the transitions to the χ_{c1} and χ_{c0} states should be detectable by experiment, whereas that to the χ_{c2} state is highly suppressed by the statistical factor \mathcal{S}_{fi} .

5.4 E1 transitions in the $b\bar{b}$ system

The number of measurable E1 transitions in the $b\bar{b}$ system is larger than in the $c\bar{c}$ system, as the $\Upsilon(3S)$ state lies below the threshold for $B\bar{B}$ fragmentation. While the branching fractions for several of the transitions presented in Table 15 have been measured, only very few of the total widths are known. This is due to the narrowness of the $b\bar{b}$ states, which makes a direct determination of their widths difficult. It is therefore instructive to compare the predicted E1 widths with those of other models, as well as with experiment. A review of the most important E1 transitions in Table 15 is given below.

Table 15: Comparison of the predictions for E1 transitions in the $b\bar{b}$ system with those of other models that use a scalar confining interaction. All widths are given in keV. The experimental widths have been extracted from ref. [10]. Note that only the branching fractions are known for most of the transitions.

	GS (ref. [3])	GZ (ref. [18])	This Work	Exp (ref. [10])
$\chi_{b2} \rightarrow \Upsilon \gamma$	33.0	33.8	36.0	$22 \pm 3\%$
$\chi_{b1} \rightarrow \Upsilon \gamma$	29.8	30.4	32.5	$35 \pm 8\%$
$\chi_{b0} \rightarrow \Upsilon \gamma$	25.7	25.3	26.6	$< 6\%$
$\Upsilon' \rightarrow \chi_{b0} \gamma$	0.73	0.76	1.01	1.7 ± 0.5 keV
$\Upsilon' \rightarrow \chi_{b1} \gamma$	1.62	1.37	1.80	3.0 ± 0.7 keV
$\Upsilon' \rightarrow \chi_{b2} \gamma$	1.84	1.45	2.03	3.1 ± 0.7 keV
$\chi'_{b2} \rightarrow \Upsilon' \gamma$	12.9	16.2	16.4	16.4 ± 2.4 %
$\chi'_{b1} \rightarrow \Upsilon' \gamma$	11.9	14.7	15.1	21 ± 4 %
$\chi'_{b0} \rightarrow \Upsilon' \gamma$	10.6	12.3	12.3	4.6 ± 2.1 %
$\chi'_{b2} \rightarrow \Upsilon \gamma$	18.2	10.4	11.4	7.1 ± 1.0 %
$\chi'_{b1} \rightarrow \Upsilon \gamma$	11.8	7.51	8.40	8.5 ± 1.3 %
$\chi'_{b0} \rightarrow \Upsilon \gamma$	6.50	3.57	4.93	0.9 ± 0.6 %
$\Upsilon'' \rightarrow \chi_{b0} \gamma$	0.114	0.029	0.15	—
$\Upsilon'' \rightarrow \chi_{b1} \gamma$	0.003	0.095	0.11	—
$\Upsilon'' \rightarrow \chi_{b2} \gamma$	0.194	0.248	0.04	—
$\Upsilon'' \rightarrow \chi'_{b0} \gamma$	1.09	1.30	1.14	1.4 ± 0.3 keV
$\Upsilon'' \rightarrow \chi'_{b1} \gamma$	2.15	2.34	2.12	3.0 ± 0.5 keV
$\Upsilon'' \rightarrow \chi'_{b2} \gamma$	2.29	2.71	2.50	3.0 ± 0.6 keV

- $\chi_{bJ} \rightarrow \Upsilon \gamma$

The calculated widths for $\chi_{bJ} \rightarrow \Upsilon \gamma$ agree rather well with those of the previous calculations presented in Table 15, although they are generally somewhat larger. The results of the present calculation suggest that the total width of the χ_{b2} state should be 164 ± 22 keV and that of the χ_{b1} 93 ± 22 keV. Similarly, the total width of the χ_{b0} is probably larger than ~ 440 keV. This situation is similar to that observed for $c\bar{c}$ [10], where the χ_{c2} is wider than the χ_{c1} by about a factor ~ 2 .

- $\Upsilon' \rightarrow \chi_{bJ} \gamma$

The largest uncertainty concerning the $\Upsilon(2S) \rightarrow \chi_{bJ} \gamma$ is the measurement of the total width of the $\Upsilon(2S)$ state. Originally given as ~ 27 keV, it now stands at 44 ± 7 keV [11]. Thus the model predictions in Table 15, which originally fitted the experimental data well, no longer do so satisfactorily. It is therefore very difficult to judge the quality of any given prediction until the experimental situation is stabilized. Still, it is noteworthy that the present calculation does give slightly better agreement with experiment than the previous models in Table 15.

- **Transitions from the χ'_{bJ} states**

The E1 transitions from the $\chi_{bJ}(2P)$ states in bottomonium provide a useful test for theoretical models since experimental data now exists on all six branching fractions [10], even though the total widths of the $\chi_{bJ}(2P)$ states are not known. The experimental results indicate that the widths for transitions to the Υ should be about one half of those for transitions to the $\Upsilon(2S)$, even though much more phase space is available for the former. Indeed, it can be seen from Table 15 that the model of ref. [3], where spin-averaged wavefunctions were employed, does not compare very well with the experimental branching fractions even though the hyperfine splittings of the $\chi_{bJ}(2P)$ states are quite small. A realistic description of these transitions requires that the hyperfine effects are accounted for by the $Q\bar{Q}$ wavefunctions, in which case the computed E1 widths agree much better with experiment.

As the calculated widths for $\chi_{bJ}(2P) \rightarrow \Upsilon(2S)\gamma$ are almost the same in ref. [18] and the present model, then it is possible to obtain realistic estimates for the total widths of the $\chi_{bJ}(2P)$ states from the measured branching fractions for the E1 transitions $\chi_{bJ}(2P) \rightarrow \Upsilon(2S)\gamma$. The width of the $\chi_{b2}(2P)$ state is then predicted to be 100 ± 15 keV, while that of the $\chi_{b1}(2P)$ is 72 ± 14 keV. The $\chi_{b0}(2P)$ state appears to be significantly broader, but because of the large errors in the reported E1 branching fractions, only a rough estimate of 267 ± 140 keV is possible.

- **Transitions from the Υ'' state**

As the reported total width of the $\Upsilon(3S)$ state [10], 26.3 ± 3.5 keV, is better known than that of the $\Upsilon(2S)$ state, then it is expected that systematic uncertainties in the reported experimental results for $\Upsilon(3S) \rightarrow \chi_{bJ}(2P)\gamma$ should be smaller than for the analogous $\Upsilon(2S) \rightarrow \chi_{bJ}\gamma$ transitions. By inspection of Table 15, it can be seen that the $\Upsilon(3S) \rightarrow \chi_{bJ}(2P)\gamma$ transitions are generally rather well described by a number of models, although the calculation of ref. [3], where spin-averaged wavefunctions were employed, appears to underpredict the empirical widths. Also, the results of ref. [18] appear to compare slightly more favorably with experiment than does the present calculation.

On the other hand, the situation concerning the $\Upsilon(3S) \rightarrow \chi_{bJ}\gamma$ transitions remains unsettled because of a strong cancellation in the E1 matrix element. As all of the models presented in Table 15 predict different widths for the $\Upsilon(3S) \rightarrow \chi_{bJ}\gamma$ transitions, then only experimental determination of the widths can settle the question. However, this may turn out to be a formidable task since all models predict widths that are an order of magnitude smaller than that of any previously measured E1 transition in the $b\bar{b}$ system. It is seen by inspection of Table 5 that the calculated widths in the E1 approximation are similar to those of ref. [3] in that the width for $\Upsilon(3S) \rightarrow \chi_{b1}\gamma$ is vanishingly small. However, the dynamical model predicts that the width for $\Upsilon(3S) \rightarrow \chi_{b0}\gamma$ should be the largest and that for $\Upsilon(3S) \rightarrow \chi_{b2}\gamma$ the smallest. It is encouraging that the same pattern is also predicted in Table 4 for the analogous transitions in the $c\bar{c}$ system, where the widths are much larger relative to the other E1 transitions. It is also noteworthy that the $\Upsilon(3S) \rightarrow \chi_{bJ}\gamma$ transitions obtain an appreciable contribution from the matrix element \mathcal{M}_2 in Table 5.

In addition to the transitions considered in Table 15, the E1 decays of the spin-singlet h_b and η_b states and the lightest spin-triplet D -wave states have also been calculated in Tables 5, 7 and 8. No empirical data exists as yet on any of these states. The pattern of E1 widths for these states is predicted to be similar to that for the analogous states in the $c\bar{c}$ system, although the widths are much smaller for $b\bar{b}$ because of the narrower wavefunctions involved.

5.5 E1 transitions in the $c\bar{b}$ system

The determination of photon momenta for E1 transitions in the bottom-charm B_c^\pm mesons has to rely completely on model predictions for the masses of the $c\bar{b}$ states. However, the uncertainty introduced by this is small, as model predictions for the major level splittings agree with each other to a large extent [5]. The results in Table 16 reveal that the predictions of the present model are similar to those obtained by ref. [5], although significant differences exist for transitions such as $B_c^*(2S) \rightarrow B_{c0}^* \gamma$ and $B_{c2}^*(2P) \rightarrow B_c^*(2S) \gamma$, where the widths are sensitive to the effects of the hyperfine components of the $Q\bar{Q}$ interaction. It is noteworthy that while the predicted widths for the $B_{cJ}^* \rightarrow B_c^* \gamma$ transitions agree rather well with those from ref. [5], there is a significant disagreement for $B_{c1} \rightarrow B_c \gamma$. When the somewhat different photon momenta are accounted for, this disagreement amounts to about a factor ~ 3 . An issue not considered in this paper is the mixing of the $L = 1$ states with $J = 1$, which is due to the antisymmetric spin-orbit interaction that was not included in the Hamiltonian (27). This mixing, which was considered in ref. [5], has the effect of allowing "spin-flip" E1 transitions of the type $B_{c1}^* \rightarrow B_c \gamma$. However, the widths for such "forbidden" transitions were found in ref. [5] to be typically suppressed by a factor ~ 100 relative to the "allowed" ones considered in this work.

Table 16: Comparison of the results for E1 transitions in the B_c^\pm ($c\bar{b}$, $b\bar{c}$) system with the predictions of ref. [5]. All widths are given in keV. In the notation B_{cJ}^* , where J is the total angular momentum, states without stars in their labels are spin singlets in the LS coupling scheme.

	EQ (ref. [5])	This Work
$B_{c2}^* \rightarrow B_c^* \gamma$	112.6	93.9
$B_{c1}^* \rightarrow B_c^* \gamma$	99.5	84.6
$B_{c0}^* \rightarrow B_c^* \gamma$	79.2	70.4
$B_c^{*'} \rightarrow B_{c0}^* \gamma$	7.8	4.22
$B_c^{*'} \rightarrow B_{c1}^* \gamma$	14.5	9.35
$B_c^{*'} \rightarrow B_{c2}^* \gamma$	17.7	12.3
$B_{c1} \rightarrow B_c \gamma$	56.4	103
$B_c' \rightarrow B_{c1} \gamma$	5.2	19.3
$B_{c2}^{*'} \rightarrow B_c^{*'} \gamma$	73.8	41.7
$B_{c1}^{*'} \rightarrow B_c^{*'} \gamma$	54.3	39.9
$B_{c0}^{*'} \rightarrow B_c^{*'} \gamma$	41.2	34.2
$B_{c2}^{*'} \rightarrow B_c^* \gamma$	25.8	32.9
$B_{c1}^{*'} \rightarrow B_c^* \gamma$	22.1	23.2
$B_{c0}^{*'} \rightarrow B_c^* \gamma$	21.9	13.4
$^3D_3 \rightarrow B_{c2}^* \gamma$	98.7	65.4
$^3D_2 \rightarrow B_{c2}^* \gamma$	24.7	15.9
$^3D_2 \rightarrow B_{c1}^* \gamma$	88.8	54.7
$^3D_1 \rightarrow B_{c2}^* \gamma$	2.7	1.61
$^3D_1 \rightarrow B_{c1}^* \gamma$	49.3	28.0
$^3D_1 \rightarrow B_{c0}^* \gamma$	88.6	45.9

As the magnetic moment operators of a $Q\bar{Q}$ system have been derived in this work, then the magnetic moment of the S -wave spin-triplet B_c^* states have been calculated as an interesting by-product. It is seen from Table 13 that the magnetic moments also receive significant corrections from the two-quark operators considered in this paper. This is not surprising since the situation is similar for the M1 decays of the $Q\bar{Q}$ systems. Inspection of Table 13 reveals that the net relativistic decrease of the B_c^* magnetic moment amounts to about 15 %, and that the exchange current contributions actually increase the net magnetic moment slightly. This situation was also noted for the M1 transition $B_c^* \rightarrow B_c \gamma$. However, because of the short-range nature of the OGE interaction, its contribution quickly becomes subdominant for the higher S -wave states. The predicted magnetic moments of the B_c^* mesons are in line with the work of ref. [23] on the magnetic moments of the baryons.

5.6 Other frameworks

The masses, radiative transitions and other properties of the heavy quarkonia have also been investigated within the frameworks of QCD sum rules [6, 7], Heavy Quark Effective Theory (HQET) [8] and Non-Relativistic QCD (NRQCD) [9]. It is of particular interest to compare the results of the present calculation with those of ref. [8], where the E1 transitions between $c\bar{c}$ and $b\bar{b}$ states were considered. The results of ref. [8] are presented in terms of an "effective" matrix element δ , from which the dependence on the angular momenta of the $Q\bar{Q}$ states and the momentum of the emitted photon has been extracted. The theoretical uncertainties are therefore concentrated into the parameter δ . As that parameter is closely related to the radial matrix element \mathcal{M}_0 for E1 decay, a direct comparison between the present work and that of ref. [8] is possible. Such a comparison is given in Table 17. In addition, the width for the E1 transitions $h_c \rightarrow \eta_c \gamma$ was in ref. [8] obtained as ~ 450 keV, which in view of the somewhat larger photon momentum of ref. [8] compares reasonably well with the present value of 370 keV.

Table 17: Comparison between the effective matrix element δ of ref. [8] and the corresponding values extracted from the present calculation. The exact definition of δ can be found in ref. [8]. Note that in the present model, the matrix element for an E1 transition also depends on the total angular momentum J , as spin-averaged wavefunctions are not employed. The reported values in this table therefore correspond to the spin average of the matrix elements given in Tables 4 and 5.

	ref. [8] [GeV^{-1}]	This Work
$\psi' \rightarrow \chi_{cJ} \gamma$	0.209 ± 0.012	0.267
$\chi_{cJ} \rightarrow J/\psi \gamma$	0.197 ± 0.012	0.215
$\Upsilon' \rightarrow \chi_{bJ} \gamma$	0.109 ± 0.009	0.086
$\Upsilon'' \rightarrow \chi'_{bJ} \gamma$	0.152 ± 0.009	0.138

5.7 Conclusions

The conclusion of this work concerning the exchange current operators and the associated two-quark E1 and M1 operators is that they play a major role in spin-flip M1 transitions, whereas they are insignificant for the E1 transitions. The reason for the smallness of the exchange charge contributions to the E1 widths is the large masses of the charm and bottom quarks, as those contributions are proportional to m^{-3} . However, as suggested in ref. [35], such operators may be significant when light (~ 400 MeV) constituent quarks are involved.

A satisfactory description of the M1 widths of charmonium was achieved in this work, under the assumption that the effective confining interaction is purely scalar. This is in line with the results of ref. [12], where the width for $J/\psi \rightarrow \eta_c \gamma$ was found to be well described by an effective scalar confining interaction within the framework of the instantaneous approximation to the Bethe-Salpeter equation. This is reassuring since it has been shown in ref. [36] that models (of equal mass quarkonia) which employ an effective linear vector confining interaction or a superposition of scalar and vector confining interactions with positive weights are inconsistent with the properties of QCD.

It should be noted that the instanton induced interaction for $Q\bar{q}$ and $Q\bar{Q}$ systems, as given by ref. [17], may also contribute a significant two-quark exchange charge operator. For light constituent quarks, such contributions may be large whereas they are much smaller for charm quarks [20]. A calculation of the associated spin-flip operators for M1 transitions could therefore provide useful and constraining information on the strength of the effective instanton induced interaction in mesons with heavy quarks.

Acknowledgments

The author expresses his thanks to Prof. Dan-Olof Riska for his valuable input on the E1 transitions, to Dr. Christina Helminen for instructive conversations concerning the derivation of the exchange charge operators, and to the Waldemar von Frenckell foundation for a fund grant during the completion of this work.

References

- [1] R. McClary and N. Byers, Phys. Rev. **D28:1692** (1983).
- [2] P. Moxhay and J.L. Rosner, Phys. Rev. **D28:1132** (1983).
- [3] H. Grotch, D.A. Owen and K.J. Sebastian, Phys. Rev. **D30:1924** (1984).
- [4] X. Zhang, K.J. Sebastian and H. Grotch, Phys. Rev. **D44:1606** (1991).
- [5] E.J. Eichten and C. Quigg, Phys. Rev. **D49:5845** (1994).
- [6] P. Colangelo, G. Nardulli and N. Paver, Z. Phys. **C75:43** (1993).
- [7] V.V. Kiselev, A.E. Kovalsky and A.K. Likhoded, Nucl. Phys. **B585:353** (2000), eprint hep-ph/0002127.
- [8] R. Casalbuoni *et al.*, Phys. Lett. **B302:95** (1993).
- [9] N. Brambilla, A. Pineda, J. Soto and A. Vairo, Nucl. Phys. **B566:275** (2000), eprint hep-ph/9907240.
- [10] D.E. Groom *et al.*, Eur. Phys. J. **C15:1** (2000) (Particle Data Group, ed. 2000).
- [11] K. Hagiwara *et al.*, Phys. Rev. **D66:010001** (2002) (Particle Data Group, ed. 2002).
- [12] J. Linde and H. Snellman, Nucl. Phys. **A619:346** (1997), eprint hep-ph/9703383.
- [13] A.V. Smilga and M.A. Shifman (ed.), *Vacuum Structure and QCD Sum Rules*, p. 490, North Holland (1992)
- [14] T.A. Lähde, C.J. Nyfält and D.O. Riska, Nucl. Phys. **A645:587** (1999), eprint hep-ph/9808438.
- [15] T.A. Lähde and D.O. Riska, Nucl. Phys. **A707:425** (2002), eprint hep-ph/0112131.
- [16] R. Blankenbecler and R. Sugar, Phys. Rev. **142:1051** (1966).
- [17] S. Chernyshev, M.A. Nowak and I. Zahed, Phys. Rev. **D53:5176** (1996), eprint hep-ph/9510326.
- [18] H. Grotch, X. Zhang and K.J. Sebastian, Phys. Rev. **D45:4337** (1992).
- [19] F. Coester and D.O. Riska, Ann. Phys. **234:141** (1994).
- [20] T.A. Lähde and D.O. Riska, Nucl. Phys. **A710:99** (2002), eprint hep-ph/0204230.

- [21] C. Helminen, Phys. Rev. **C59:2829** (1999), eprint hep-ph/9711252.
- [22] K. Tsushima, D.O. Riska and P.G. Blunden, Nucl. Phys. **A559:543** (1993).
- [23] K. Dannbom, L.Ya. Glozman, C. Helminen and D.O. Riska, Nucl. Phys. **A616:555** (1997), eprint hep-ph/9610384.
- [24] C. Helminen, Univ. of Helsinki Rep. Series in Phys. **HU-P-D81** (2000),
<http://ethesis.helsinki.fi/julkaisut/mat/fysii/vk/helminen/>
- [25] A.C. Mattingly and P.M. Stevenson, Phys. Rev. **D49:437** (1994), eprint hep-ph/9307266.
- [26] P.A. Movilla-Fernández, S. Bethke, O. Biebel and S. Kluth, Eur. Phys. J. **C22:1** (2001), eprint hep-ex/0105059.
- [27] S.K. Choi *et al.*, (BELLE Coll.) Phys. Rev. Lett. **89:102001** (2002), eprint hep-ex/0206002.
- [28] F. Abe *et al.*, (CDF Coll.) Phys. Rev. Lett. **81:2432** (1998), eprint hep-ex/9805034.
- [29] Y.-Q. Chen and Y.-P. Kuang, Phys. Rev. **D46:1165** (1992).
- [30] J. Zeng, J.W. Van Orden and W. Roberts, Phys. Rev. **D52:5229** (1995), eprint hep-ph/9412269.
- [31] S. Godfrey and N. Isgur, Phys. Rev. **D32:189** (1985).
- [32] S.N. Gupta, W.W. Repko and C.J. Suchyta III, Phys. Rev. **D39:974** (1989).
- [33] H. Grotch, K.J. Sebastian and X. Zhang, Phys. Rev. **D49:1639** (1994).
- [34] E. Eichten *et al.*, Phys. Rev. **D21:203** (1980), Phys. Rev. **D17:3090** (1978).
- [35] K.O.E. Henriksson *et al.*, Nucl. Phys. **A686:355** (2001), eprint hep-ph/0009095.
- [36] D. Gromes, Phys. Lett. **B202:262** (1988)